2

NATIONAL AERONAUTICS AND SPACE ADMINISTRATION

Technical Memorandum 33-522

ATS-5 Solar Cell Experiment Results After One Year in Synchronous Orbit

B. E. Anspaugh

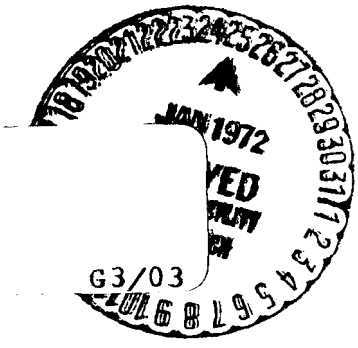

JET PROPULSION LABORATORY
CALIFORNIA INSTITUTE OF TECHNOLOGY
PASADENA, CALIFORNIA

January 1, 1972

47

NATIONAL AERONAUTICS AND SPACE ADMINISTRATION

Technical Memorandum 33-522

ATS-5 Solar Cell Experiment Results After One Year in Synchronous Orbit

B. E. Anspaugh

JET PROPULSION LABORATORY
CALIFORNIA INSTITUTE OF TECHNOLOGY
PASADENA, CALIFORNIA

January 1, 1972

Prepared Under Contract No. NAS 7-100
National Aeronautics and Space Administration

PREFACE

The work described in this report was performed by the Guidance and Control Division of the Jet Propulsion Laboratory.

ACKNOWLEDGEMENTS

The author wishes to acknowledge the enormous help given him in this work. The people at Hughes Aircraft Company who contributed the major design and construction tasks were A. Burstein, W. Dawson, W. Dunkerly, L. Goldhammer, C. Agnew, R. Sklar, R. Julian and A. Gardner. NASA Headquarters personnel who have actively lent their support are: A. Smith, D. Novik, and W. Woodward. Those at Goddard Space Flight Center who have assisted particularly are R. Darcey, D. Fordyce, and J. Wagner of the ATS Project Office and E. Metzger, J. Day, R. Moore, G. Repass, and P. McKowan who operate the experiment, and record the raw data and supply ephemeris data. JPL personnel who contributed generously were A. Briglio, W. Collier, D. Runkle, and J. Goldsmith who assisted with their managerial talents; R. Yasui, R. Mueller, and W. Wall who at one point rescued the entire program by designing, building, and testing one of the experimental solar panels; R. Prizgintas who wrote and debugged many computer programs; and S. Joines who ran the programs.

CONTENTS

FIGURES (contd)

ABSTRACT

The results of the ATS-5 solar cell experiment after one year in synchronous orbit are reported. A partial failure in the experimental electronics package has caused a loss of data from half the 80 experimental solar cells. Procedures for extracting data due to a partial spacecraft failure are described and discussed. Data from the remaining 40 solar cells, including 15 mounted on a thin flexible structure are analyzed. Data are corrected to a solar intensity of 140 mW/cm^2 and a temperature of 25 °C.

It was found that after one year in synchronous orbit: (1) cells with 1.52-mm-thick coverslides did not show a clear-cut advantage over those with 0.15-mm coverslides, (2) cells with solderless grid lines are degrading at the same rate as are cells with solder-dipped grid lines, (3) cells not quite completely covered with coverslides suffered a large power loss in comparison to cells fully covered, (4) no clear-cut advantage of 10-Ω-cm cells over 2-Ω-cm cells has yet been observed, (5) cells mounted on the flexible panel with relatively little backshielding did not degrade any faster than those with substantial backshielding, and (6) the flight data in large part confirms the adequacy of the ground-based techniques used in our pre-flight radiation test program.

I. INTRODUCTION

Solar cells today remain the prime source of power for unmanned spacecraft, both Earth-orbiting satellites and interplanetary vehicles. The cells are almost exclusively silicon chips 2 × 2 cm square with a junction very near the front or sunward surface. Since the junction must be near the surface to allow the penetration of sunlight to generate hole-electron pairs near the junction, the junction is, in turn, very susceptible to damage by energetic electrons and protons. Such junction damage results in a loss of power output and ultimately will lead to the failure of the spacecraft. There is a continuing effort to fabricate cells of higher efficiency consistent with radiation resistance and to protect them with materials (usually quartz coverslides) having minimum weight. Testing of developmental cells and protective materials is accomplished by a series of laboratory tests, including irradiation with particle accelerators, and by flying them on satellites. Since it is always difficult, if not impossible, to properly simulate the complex space environment, including electrons, protons, and ultraviolet radiation, temperature cycling and hard vacuum in the laboratory, the ultimate and final test must be an actual spaceflight to determine cell behavior. The goal of this experiment is to assess the behavior of several selected cell types and coverslides in the equatorial synchronous orbit region.

The ATS-5 satellite was launched into synchronous orbit on August 12, 1969. The spacecraft attitude-control method was to be gravity gradient stabilization with a resulting spin rate of one revolution per day. The solar cell experiment, aboard the spacecraft, incorporated two solar panels which were to rotate into normal incidence with the Sun once a day. An unfortunate chain of circumstances occurring soon after launch resulted in the satellite going into a fast spin about the proper axis but in the wrong direction. The spacecraft could not be de-spun to a rate considered safe for extending the

gravity gradient booms. Many of the mission objectives were found to be partially attainable with spin, so the decision was made to leave the spacecraft in its spinning state rather than risk additional problems by attempting to extend the booms. However the method of data extraction from the experiment had to be modified, and a revised operations plan for the solar cell experiment was put into effect 83 days after launch. The revised plan was found satisfactory, and data has been received, but at the expense of a slight loss in accuracy.

II. EXPERIMENT OBJECTIVES

The ATS-5 solar cell radiation experiment was designed to isolate, correlate, and identify the mechanisms responsible for solar cell degradation in a radiation environment. Specific objectives were as follows:

1. Compare radiation susceptibility of two types of lithium-doped solar cells with solar cells of current standard design.
2. Correlate the observed radiation degradation with the radiation environment as measured by the radiation spectrometers on the spacecraft.
3. Correlate the measured flight effects with data from the ground test program and verify the ground-based testing techniques and facilities.
4. Correlate radiation effects with the thickness of the protective coverslides.
5. Study coverslide or adhesive darkening caused by ultraviolet and particulate radiation or in-flight deposition of debris on the coverslides.
6. Study cell degradation resulting from low-energy proton damage to exposed solar cell areas and contacts.
7. Study radiation effects of cells whose rear surfaces were protected with minimal shielding.
8. Identify cell degradation as a function of the presence or absence of solder coating on the cell contact strips and grid lines.

To fulfill these objectives, the experimental solar panels were constructed with the combinations of solar cells and coverslides shown in Table 1. Each combination or configuration listed is made up of five samples. The configurations shown in grey in Table 1 are the samples serviced by signal processor unit (SPU) No. 2. Since this signal processor failed shortly after launch, no data is received from half the solar cells. The original objectives are still attainable, with the exception of Nos. 1 and 5. The others are compromised to some extent but meaningful data can still be extracted.

III. EXPERIMENT DESIGN

Flight Hardware

Sixty-five solar cells are mounted on a rigid panel and fifteen on a flexible panel. Two signal processors independently measure twelve current-voltage pairs of forty solar cells and the temperature of eight thermistors embedded in the panels. The location of the solar panels and signal processor units on the ATS-5 spacecraft is shown in Fig. 1. The rigid panel (Fig. 2), constructed of aluminum honeycomb, is tangentially mounted on the spacecraft midsection, and the flexible panel (Fig. 3) is radially mounted on the spacecraft midsection. The flexible panel substrate consists of a ply of 0.025 mm (0.001 in.) Dupont Kapton H-film bonded to a ply of 0.025 mm (0.001 in.) type 108 fiberglass scrimcloth. The protruding position of the panel and the thin substrate backing allow radiation to impinge relatively unimpeded on the rear of the cells mounted on the flexible panel. The cell configurations mounted on this panel are repeated on the rigid panel to distinguish the effects of rear-incident radiation.

On the rigid panel the cells are mounted, in groups of five, on independent titanium strips bonded to the panel (Fig. 4). Each five-cell group on a strip represents one of the cell configurations selected for this experiment. A thermistor is mounted in the rigid panel just beneath the center of each titanium strip to monitor the module temperature. The rigid panel measures 31.4 cm × 34.00 cm × 3.65 cm, including the connector, and weighs 0.993 kg. The flexible panel measures 24.21 cm × 13.98 cm × 9.50 cm and weighs 0.299 kg. The panels are mounted in the central bellyband area of the spacecraft.

The two electronic signal processing units are stacked on the spacecraft aft bulkhead. Each signal processor weighs 1.088 kg, consumes 3.3 W of power, and measures 13.21 cm × 22.86 cm × 3.05 cm. Each signal processor contains 399 discrete components, 80 integrated circuits, and 51 relays. The integrated circuits and small discrete components are packaged on a "stick" called a MICAM (micro connection assembly method) and are encapsulated in protective foam after assembly and functional verification. The major discrete components are housed in welded cordwood modules and coated with an epoxy conformal coating. The signal

processors are powered by a single spacecraft payload regulator. The experiment is turned on and off by a ground command which controls the payload regulator. Each signal processor must perform five tasks:

1. Select each cell in sequence, then switch 12 resistive loads in sequence across the selected cell.
2. Measure the cell voltage and output current for each load and amplify these signals to a level acceptable for spacecraft encoder input.
3. Generate signals which identify the cell being measured.
4. Measure the temperature of each 5-cell module.
5. Periodically insert calibration voltages into each amplifier input for continuous amplifier calibration.

In addition to reading out the output of the solar cells in the experiment, the signal processors also are used to read out several spacecraft temperatures. Since the data multiplexing scheme used by the signal processing units allowed room for a few additional readouts, a number of spacecraft bellyband and solar panel temperatures were processed through these units. Also monitored are the temperatures of the signal processing units themselves, allowing temperature corrections to be made to the solar cell load resistances.

Signal processor unit (SPU) No. 2 failed at some time between launch and the first activation of the experiment on Sept. 6, 1969, causing loss of data from half the solar cells. Data continues to be acceptable from the other half of the solar cells.

IV. EXPERIMENT OPERATION

The current vs voltage (I-V) curve of each solar cell is measured by connecting, in turn, 12 precisely known resistive loads across the cell. A four-point connection to each cell is used for enhanced accuracy, since a non-negligible and variable voltage drop occurs in the wiring harness, the relay contacts, and the connectors. In operation, each SPU selects a cell, then sequentially switches each of the 12 load resistors across that cell. Load switching is also done by relay, using DPDT relays with the contacts in parallel for lowest possible contact resistance. After load switching for a cell is complete, four more voltages of a varied nature are multiplexed onto certain spacecraft telemetry channels prior to selection of a new cell. These signals include four calibration voltages to establish amplifier gain in both and current channels, solar cell temperature, SPU temperature, major frame identification voltages, an output signal with input shorted, and spacecraft panel and bellyband temperatures. A major frame in this experiment consists of the complete complement of telemetry signals for four solar cells.

The signal processing units each supply a voltage signal, a current signal, and the housekeeping signals to both of the two spacecraft data encoders. The signal processing units operate independently, each stepping through its own cells, generating its own cell identification and calibration voltages, etc., and sending all the voltages to the spacecraft encoder in the proper sequence. The 40 cells monitored by each SPU are divided into 10 major frames of 4 cells each. SPU 1 sends the cell voltages to spacecraft telemetry channel 29 and the cell current signals to channel 30 by way of the encoders. Each time SPU 1 selects a new major frame, bit 3 in channel 14 changes state from a logical 1 to a logical 0. The voltage and current channels for SPU 2 are 42 and 57, respectively, and bit 4 of channel 14 is used for its major frame indication. Bit 9 of channel 14 is used to indicate the on/off status of the payload regulator.

There are 64 spacecraft telemetry channels. The experiment uses 4 of these channels and a portion of a fifth. During normal operation all 64 channels are transmitted sequentially, each complete readout requiring approximately 2.9664 sec. As the encoder steps through channel 0 each

time, a pulse is sent to each SPU. The encoder channel 0 pulse is used to time all the internal SPU switching. An example will illustrate the operational sequence. At experiment turn on (by ground command) SPU 1 may begin with load 4 connected to cell 0. (Readout sequence does not begin with any particular cell or load). The voltage and current levels appropriate to cell 0, load 4 are telemetered via channels 29 and 30, respectively, during the ensuing telemetry frame. A channel 0 pulse signals the beginning of the next telemetry frame and switches load 5 to cell 0, setting up a new pair of cell voltage and current levels which in turn are transmitted through channels 29 and 30. The switching continues for loads 6 through 11 each time the channel 0 pulse steps the SPU. Following readout of the eleventh cell load the 8 housekeeping signals are then selected in turn, four being routed through voltage channel 29 and four through current channel 30. Switching of these signals is also timed by the channel 0 pulse. The next channel 0 pulse will select cell 1 and connect load 0 and the sequence continues stepping through all cells and loads. After the cell 39 readout is complete, the entire sequence is repeated starting with cell 0, load 0. At the same time, SPU 2 is performing the same steps with cells 40 through 79 and telemetering the signals through channels 42 and 57. The channel 0 pulse is also used to step SPU 2.

SPU 1 and SPU 2 operate simultaneously and the total experiment readout time is

$$2.966 \frac{\text{sec}}{\text{frame}} \times \frac{16 \text{ frames}}{\text{solar cell}} \times 40 \text{ solar cells} \times \frac{1}{60} \frac{\text{min}}{\text{sec}} = 31.6 \text{ min}$$

The spacecraft in gravity gradient stabilization would rotate approximately

$$\frac{360 \text{ deg}}{\text{day}} \times \frac{1 \text{ day}}{1440 \text{ min}} \times 31.6 \text{ min} = 7.9 \text{ deg}$$

The turn-on timing was to be such that Sun-normal for the rigid panel would occur midway in the readout so the maximum angle of incidence would be 4 deg (cos 4 deg = 0.998). The rigid panel normal is parallel with spacecraft $\theta = 267°16'$ and the flexible panel normal is parallel with spacecraft $\theta = 214°6'$ (Fig. 1). This geometry would require two turn-on times, 3 h, 32 min apart to achieve Sun normal to both panels.

This plan was abandoned when the spacecraft ended up spinning permanently at 76 rpm (0.788 sec/rev). Fortunately the ATS spacecraft has an

alternative telemetry mode available called dwell mode. In dwell mode operation, the spacecraft encoder can be locked on to a particular telemetry channel and data from that channel only will be transmitted. Data from that channel is sampled at a rate 64 times higher than during normal mode operation (every 0.04635 sec versus every 2.966 sec). The spacecraft encoder can therefore be commanded to dwell on voltage channel 29, and here one can observe the voltage output of any given solar cell connected to one of the loads cycle up and down as the spacecraft rotates the panels through Sun normal and into occultation (Fig. 5). The same can be seen by dwelling on current channel 30. Assuming the maxima coincide with the Sun normal, one has only to sort through this dwell-mode data and extract maximum values for each cell/load combination. Problems remaining are cell and load identification and matching voltage data to current data. In the format all cell identification information rides on the voltage channel. No channel 0 pulse is furnished by an encoder operating in dwell mode, therefore a pulse must be provided from an alternate source for stepping the electronics. These problems were resolved by running the other spacecraft encoder in the normal mode simultaneously. This encoder supplies the needed channel 0 pulse and furnishes the cell identification signals. The two sets of data, normal and dwell, are telemetered simultaneously and recorded in parallel. They can be merged and correlated at a later time, since the time of day is recorded (to a resolution of 1 ms) on each tape at the beginning of each spacecraft telemetry frame.

The data processing must now identify the block of dwell data for a given cell and load, then select the data points corresponding to the time of nearest normal incidence. The spacecraft will rotate 21.2 deg between dwell data points at its present rate of rotation. If the maximum point in the block of dwell data were selected and assumed to be the time of normal solar incidence, the result could be off a maximum of 10.6 deg from true normal incidence. This introduces an error of no more than 1.7% in the estimate of the incident intensity. Maxima are selected for the cell voltages and also for the cell currents. Using the normal data and the time, the voltages are paired with their corresponding currents for all cells and loads to give entire I-V curves for each cell.

Data Processing

The cell I-V curves are generated as described in the previous section using a Univac 1108. The next data processing level consists of: (1) computing the gain and offset of the voltage and current amplifiers using the 4 calibration voltage outputs from each, (2) computing the cell temperatures for each group of 5 solar cells, and (3) computing the voltage and current at the solar cell using the calculated gains and known values of the load resistors. Data from the 1108 computer in the form of punched cards is put into the IBM 1620 where the above steps take place and I-V curves are also plotted. As an extra check, the series resistance due to cable resistance, connector contact resistance, and relay contact resistance is calculated ($[V/I] - R_L$) and scanned to check for relay malfunction and for bad data points. Typically this series resistance has values of between 0.3 to 0.7 Ω, is not constant, and emphasizes the necessity for using the 4-wire measurement technique.

The resulting I-V curves are examined manually for the purpose of determining trends, finding bad data points, and finding values of short-circuit current I_{sc}, open-circuit voltage V_{oc}, current at maximum power I_{mp}, and voltage at maximum power V_{mp}. At this point the solar intensity incident on the cells is found by calculating spacecraft to Sun distance and spacecraft axis tilt angle from the ATS-5 ephemeris data tapes furnished by GSFC. These data together with cell temperature are now used in a final calculation to compute averages, standard deviations, and 95% confidence limits of I_{sc}, I_{sc}/I_{sco}, V_{oc}, V_{oc}/V_{oco}, I_{mp}, I_{mp}/I_{mpo}, V_{mp}, V_{mp}/V_{mpo}, P_m, and P_m/P_{mo} for each set of 5 cells comprising a configuration of Table 1. The "o" subscripts refer to preflight cell measurements at 140 mW/cm^2, 25°C with the X-25 solar simulator. The flight data are corrected to values corresponding to 140 mW/cm^2 and to 25°C. Statistical parameters for the corrected data are also calculated.

The method of performing temperature and intensity calculations is based on a curve fit (Ref. 1) to the data of Yasui (Ref. 2) and Sandstrom (Ref. 3). The corrections used are as follows:

$$I_{sc}(T_2, I_2) - I_{sc}(T_1, I_1) = c(I_2 - I_1) + d(I_2T_2 - I_1T_1)$$

$$P_m(T_2, I_2) - P_m(T_1, I_1) = a(I_2 - I_1) + b(I_2T_2 - I_1T_1)$$

$$V_{oc}(T_2, I_2) - V_{oc}(T_1, I_1) = e(T_2 - T_1) + f(\log I_2 - \log I_1) + g(T_2 \log I_2 - T_1 \log I_1)$$

where

T_2 = reference temperature (25°C)

T_1 = cell temperature

I_2 = reference solar intensity (140 mW/cm^2)

I_1 = solar intensity on the cells.

The coefficients a through g depend on the resistivity of the solar cell. Their values are as shown in Table 2.

Solar intensity incident on the panels is derived from ATS-5 ephemeris data. A plot of the spacecraft-Sun distance and spacecraft tilt angle is plotted in Fig. 6 as a function of time for 1969 and 1970. The data shown are for midnight, UMT. The intensity on the solar cells is calculated by

$$I = \frac{140 \cos \theta}{\left(\frac{d}{d_0}\right)^2} \text{ mW/cm}^2$$

where d is the spacecraft-Sun distance and d_o is 1 AU (= 1.49599×10^8 km). It has been found (Ref. 1) that the cosine function gives a very good (< 1% error) representation of the intensity incident on a tilted panel for tilt angles up to 45 deg.

A set of I-V curves for cells 36 through 39 is shown in Figs. 7 and 8. The Fig. 7 curves are taken prior to mounting the cells on the panel. Figure 8 depicts the I-V curve data as received from the spacecraft on August 10, 1970, 363 days after launch. Temperature and solar intensity corrections were not made on the curves shown. At the time these curves were taken the solar intensity at the panel was 132 mW/cm^2 and the cell

temperature was -0.9°C. The corrections to bring the cells to 140 mW/cm^2 and 25°C were approximately +11.2 mA in I_{sc}, -54.6 mV in V_{oc}, and -4.0 mW in P_{max}. Similar sets of I-V curves are generated each time the experiment is activated. Temperature corrected average values for each set of five similar cells are given for I_{sc} in Figs. 9-11, for P_{max} in Figs. 12-14, and for V_{oc} in Figs. 15-17.

The prefabrication cell data using an X-25 solar simulator was selected for use as the preflight reference because the cell temperature was tightly controlled at that time. Figures 9-17 show post-fabrication values also for I_{sc}, V_{oc} and P_{max}, where the entire panel was illuminated by the solar simulator for the I-V curves. However, the panel temperature at measurement was nominally 50°C rather than 25°C. Examination of the V_{oc} data, particularly for cells 0-14 on the flexible panel, reveals that the temperature was not stable during the measurements and the data must be viewed as questionable. Therefore it was decided that use of the prefabrication data, even though the coverslides were not yet mounted, would be the most accurate baseline. This uncertainty and the spacecraft failure that precluded early post-launch data, which could have been used for baseline data, has led to the use of only absolute values for the solar cell parameters in this report.

The I-V curves of Fig. 8 point up another interesting anomaly in the flight data. The first load typically gives a current that appears to be too high. The second load current usually appears too low, and on occasion the third load current also appears low. The terms "low" and "high" are in reference to the nearly constant current portion of the usual I-V curve below 0.3 V (see Fig. 7). The reason for this behavior is not conclusively known. Most probably it is due to inaccuracy of the signal-processing unit at the low voltage end. I_{sc} values are derived from these curves by simply picking the current corresponding to one of the first four loads which is felt to best represent the averaged extrapolation to zero voltage. A least-square linear fit to the first four load points was calculated and extrapolated to zero voltage, but the "eyeball" method generally gave more reasonable values because the high currents associated with load zero usually influenced the fit to give a highly negative slope and high values for I_{sc}. Because this procedure of extracting I_{sc} does insert a certain degree of subjectivity into the

I_{sc} data, most of the observations and conclusions will be made on the basis of the maximum power output of the cells.

Figure 18 compares the maximum power output of four solar cell configurations which are identical except for different coverslide thicknesses. These values have been corrected for temperature and solar intensity. Each point depicted is an average of five cells. After 363 days in orbit the ranking in power output from maximum to minimum by coverslide thickness is 0.30 mm (12 mil), 0.15 mm (6 mil), 1.52 mm (60 mil) and 0.51 mm (20 mil). This is not the expected order, particularly when one considers that the cells bearing 0.30- and 0.15-mm coverslides are mounted on the flexible panel and subject to irradiation from the rear. Statistical tests were performed to determine if the difference noted is significant. Statistical comparison consists of two steps: (1) At the 5% significance level use an equal-tails F test to determine whether the two sets of data have equal standard deviations, and (2) If so, use an equal-tails t-test at the 5% significance level to test for differences in the average values (Ref. 4). Here the highest output cells (0.30-mm coverslide) were compared with the lowest output cells (0.51-mm coverslide) and it was found that there is no statistically significant difference in the power output of these cells. After one year in space the 0.15-mm coverslides are giving as much protection to the cells as are coverslides ten times as thick. The same comparison is made in Fig. 19, plotting I_{sc} average values. Here the thicker coverslides are giving slightly higher currents, but again there is no difference in a statistical sense between the high and low values. The preflight accelerator tests showed a rather clearcut advantage to using thicker coverslides, after an "equivalent" 5-year exposure, but the standard deviations of the flight data are still too large in comparison to the interconfiguration averages to determine the best protective coverslide thickness.

Figure 20 compares the average P_{max} values for solar cells otherwise identical except for grid line fabrication. Cells 20-24 have solderless grid lines, but cells 15-19 have solder-dipped grid lines. These cells all have 1.52-mm coverslides. The P_{max} for the solderless gridline cells is higher from prefabrication through 363 days space exposure. Application of the statistical t-test confirms that the difference is real.

Figure 21 is a comparison plot of the P_{max} values for cells 0.30 mm thick and covered with 0.30-mm coverslides with a solderless busbar, with a solder dipped busbar, with a 0.38-mm gap in the coverslide coverage near the busbar and of cells with a 0.43-mm busbar gap irradiated in the laboratory (Ref. 5). The last group of cells were irradiated with a spectrum of protons tailored to match the energy and fluence of one year in synchronous orbit, and further corrected for the effect of one year exposure to the synchronous orbit electron spectrum. Here the behavior of the solderless busbar and solder-dipped busbar is nearly identical. In contrast, the gap cells degraded very rapidly by the 83rd day in orbit and gradually thereafter. The laboratory-irradiated cells do not appear to follow the flight cells at all in rate of power loss.

Figures 22 and 23 show the I_{sc} and V_{oc} data for the same flight cells as shown in Fig. 21. It is evident that the difference in cell power output is due to reduction in V_{oc}, while the I_{sc} values change only slightly. This is characteristic of cells with incomplete coverslide coverage when irradiated with low-energy protons and the resultant damage to the cell junction. If electron radiation had been the primary agent, there would have been a falloff in the short-circuit current as well. If it had been due to debris on the coverslide or to darkening of either adhesive or coverslide, it would have shown up on all cells and affected I_{sc} primarily and left V_{oc} relatively unscathed. The cause of such a rapid degradation of the "gap" cells shortly after launch is not yet known. Data from the radiation spectrometer experiment aboard ATS-5 will soon be available and will be examined to see if any unusual low-energy proton event occurred during the time period in question. In comparing the solderless busbar cells with the soldered busbar cells, there is no apparent difference in the maximum power output. Yet Fig. 23 does show that the open-circuit voltage is dropping faster for the solderless busbar cells, and after a year the difference is significant. Since a solderless busbar is very similar to a cell with a coverslide gap, this trend is not surprising. In time the voltage drop will probably be reflected in a cell power loss. In any event, this result clearly points out the importance of carefully shielding all solar cells completely, including the busbar, if they are to be flown in a radiation environment.

Figure 24 compares the average maximum power output of the three cell configurations on the flexible panel. After one year there is not yet any significant difference in the power output of any of the three types. The trend is for the 10 Ω-cm cells to perform slightly better than the 2 Ω-cm cells, but later data will be required to substantiate any such superiority.

Figures 25 and 26 compare ground test radiation data with flight data for cells protected with 0.15-, 0.30- and 1.52-mm coverslides. The ground test radiations were carried out with the JPL Dynamitron accelerator with the cells mounted on a rotating aluminum cylinder (Refs. 5 and 6). Three electron energies of 0.5, 0.7, and 1.0 MeV were used in turn together with suitable scattering foils and air scattering to closely simulate the Van Allen belt electron spectrum at synchronous orbit altitude. Radiation fluences were given to the cells designed to simulate 0.25, 0.5, 1.0, and 5.0 years radiation dose in synchronous orbit. After each exposure the cells were removed from the aluminum cylinder and I-V curves taken using the JPL X-25L solar simulator with cell temperature 25 ±0.5°C.

The comparison of flight vs ground test in Fig. 25 for the average maximum power of cells with 0.15-mm coverslides shows a large disparity throughout the test. This is largely due to a lower starting average power of the ground test cells. By ratioing the power to the pretest levels, it is found that after one year the flight cells have a reduction of 6% and the accelerator irradiated cells a reduction of 7%, so the agreement is quite good using normalized values.

Comparison with cells having 1.52-mm coverslides reveals a different problem. Here the ground test and flight data had a moderate disparity in their starting points, but the flight cells degraded much faster than did the laboratory cells. Both sets of cells arrived at very nearly the same end point after one year, but their degradation rates do not appear to have the same slope. Cells in flight with the thick coverglass appear to be degrading at a higher than expected rate ($P/P_o = 0.92$), but most of the loss occurred between the initial point and the first flight data readout. Recalling that the initial data points for the flight cells are solar simulator data taken prior to mounting the coverslides, it is possible that the cell output change seen here may be in some part due to coverslide mounting and contact soldering.

Ground test and flight cells with 0.30-mm coverslides behaved almost identically. They each degraded at approximately the same rate with time, had similar starting and ending points, and after one year had each degraded 5% in maximum power.

V. CONCLUSIONS

1. After one year in orbit, cells protected with 0.15-mm coverslides have as much power output as cells protected with 1.52-mm coverslides. One year's exposure to the synchronous orbit radiation environment is not enough to show significant differences.

2. Cells with solderless grid lines are degrading at the same rate as are cells with solder-dipped grid lines.

3. Incompletely covered cells lose maximum power and open-circuit voltage much faster than completely covered cells, giving full confirmation to analysis and ground test results.

4. Ten Ω-cm cells are exhibiting slightly less power loss than are 2 Ω-cm cells, but the difference is not yet significant.

5. Cells on the flexible panel are not degrading faster than the cells on the rigid panel, showing that radiation incident on the rear surfaces of solar cells is not a serious problem after one year in this environment.

6. Agreement between in-flight and ground-based accelerator and simulator testing is quite good, confirming adequacy of the laboratory analysis, facilities, and test procedures.

REFERENCES

1. Anspaugh, B. E., "Solar Cell Output as a Function of Temperature and Illumination Angle-Of-Incidence," Technical Memorandum 33-495. Jet Propulsion Laboratory, Pasadena, California, Sept. 1971.

2. Yasui, R. K., unpublished experimental data, Jet Propulsion Laboratory Photovoltaics Group, October, 1970.

3. Sandstrom, J. D., "Electrical Characteristics of Silicon Solar Cells as a Function of Cell Temperature and Solar Intensity," Proceedings of the IECEC Conference, Boulder, Colorado, August, 1968

4. Crow, E. L., Davis, F. A., Maxfield, M. A., "Statistics Manual," Dover Publications, Inc., New York, N. Y., 1960.

5. Dawson, W. P., and Goldhammer, L. J., "Solar Cell Radiation Flight Experiment," Final Report, JPL Contract 952351, May 30, 1969.

6. Goldhammer, L. J., and Anspaugh, B. E., "Electron Spectrum Irridiations of Silicon Solar Cells," Proceedings of the Eighth IEEE Photovoltaic Specialists Conference, Seattle, Washington, August, 1970.

Table 1. Experimental solar cell configurations

Configuration No.	Cell Nos.	SPU	Special characteristics*	Resistivity (Ω-cm)	Cell thickness (mm)	Coverslide thickness (mm)	Panel location (F = Flexible R = Rigid)
1	45-49	2	No optical coating on coverslide	10	.30	.30	R
2	40-44	2		10	.30	.15	R
3	55-59	2		10	.30	.30	R
4	25-29	1		10	.30	.51	R
5	15-19	1		10	.30	1.52	R
6	50-54	2	p/n type, Li float zone		.30	.15	R
7	60-64	2	p/n type, Li crucible		.30	.15	R
8	30-34	1	Solderless bar contact	10	.30	.30	R
9	35-39	1	0.38 mm strip unprotected by coverslide	10	.30	.30	R
10	65-69	2		2	.20	.15	R
11	10-14	1		2	.20	.15	F
12	75-79	2	0.13 mm strip unprotected by coverslide	10	.30	.30	R
13	0-4	1		10	.30	.30	F
14	5-9	1		10	.30	.15	F
15	20-24	1	Solderless grid lines	10	.30	1.52	R
16	70-74	2	No coverslide optical coating or adhesive. Cells heavily pre-irradiated	10	.30	.30	R

*All configurations with the exception of 6 and 7 are of the n/p type.

Table 2. Temperature-intensity coefficients for 2-Ω-cm and 10-Ω-cm n/p solar cells

Cell resistivity		
Coefficient	10 Ω-cm	2 Ω-cm
a	0.465	0.440
b	-0.00209	-0.00172
c	1.004	0.870
d	0.000977	0.000582
e	-2.972	-2.600
f	42.4	63.85
g	0.383	0.231

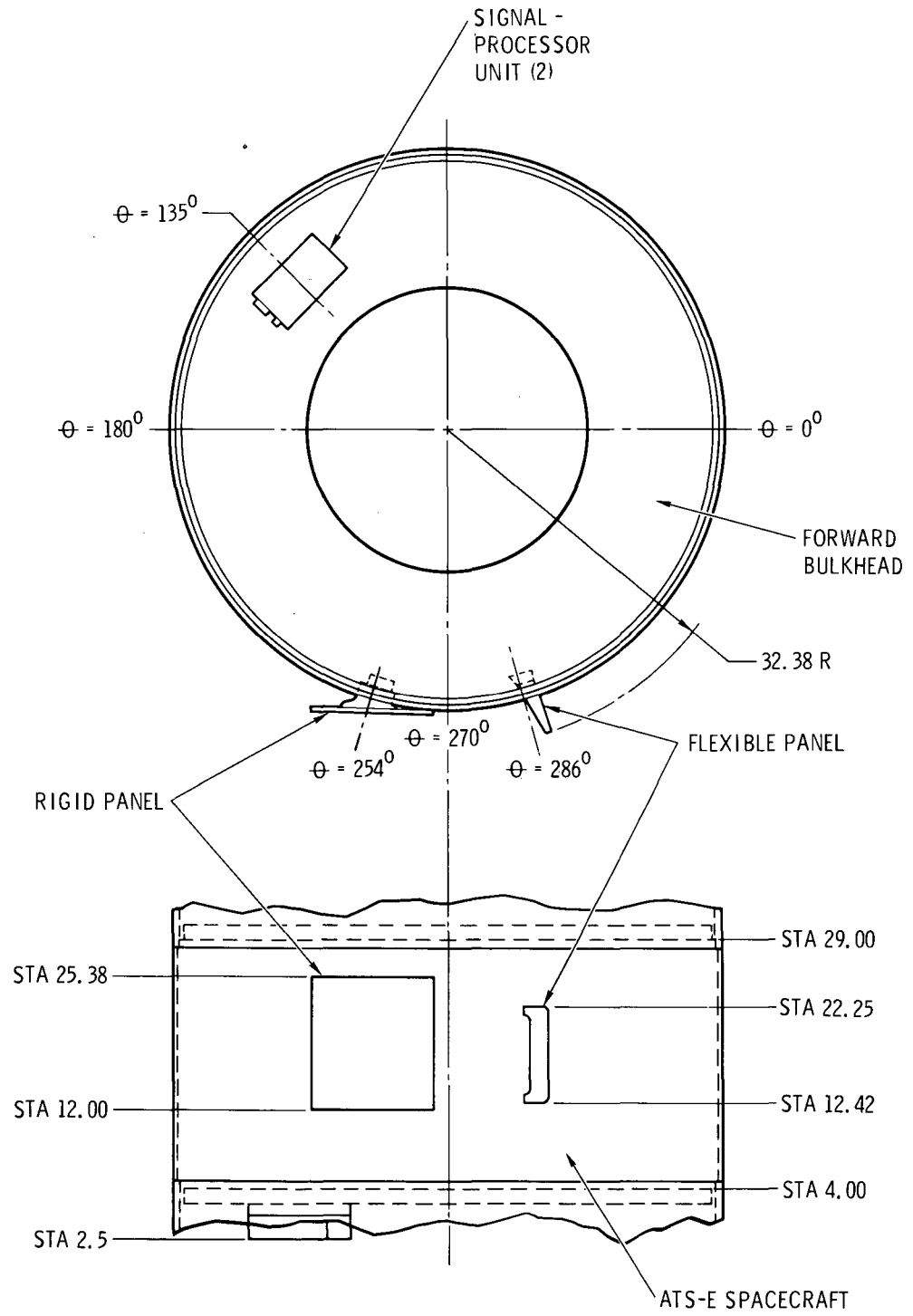

Fig. 1. Solar cell experiment locations on ATS-5 spacecraft

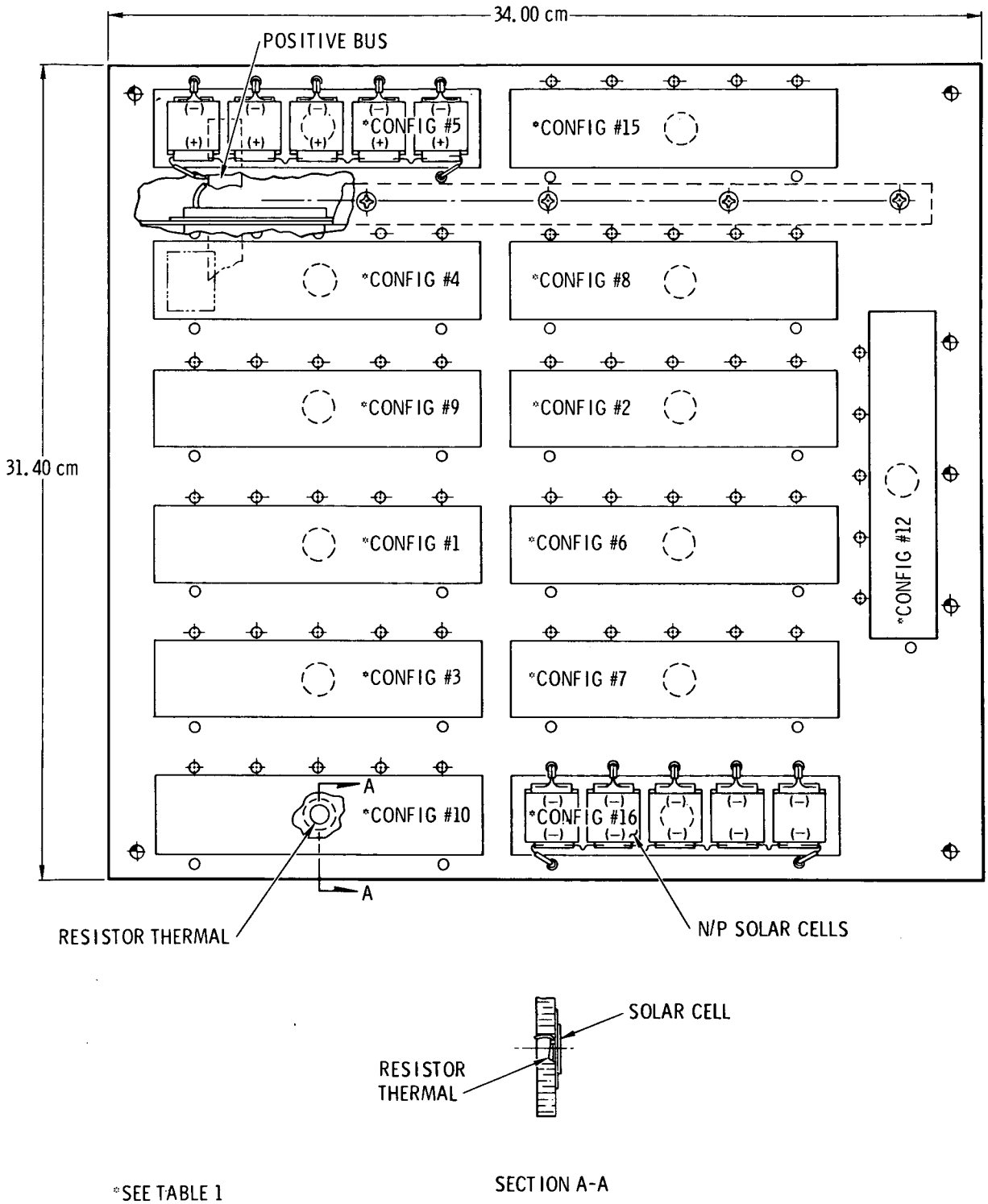

*SEE TABLE 1

Fig. 2. Layout of rigid solar panel

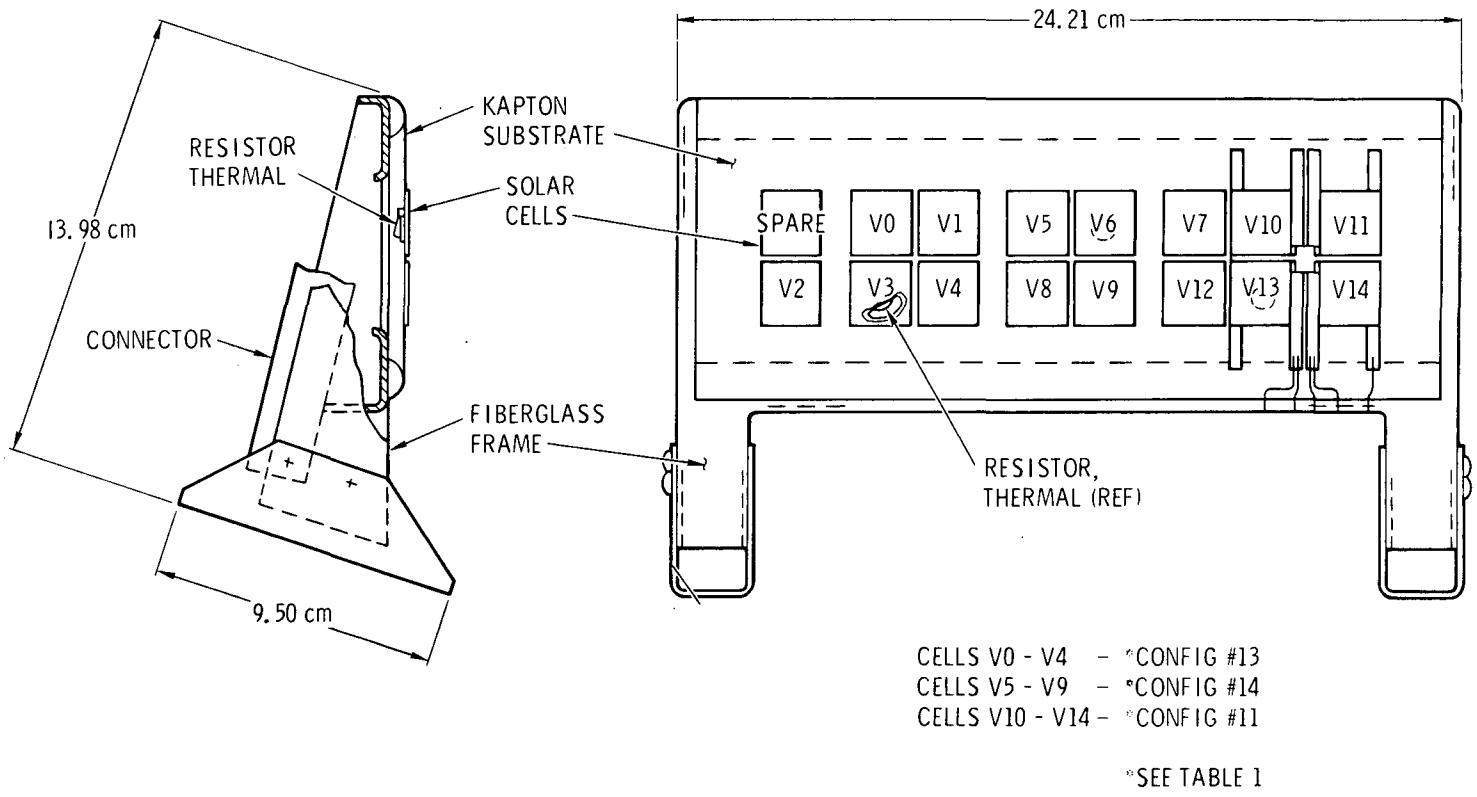

Fig. 3. Layout of flexible solar panel

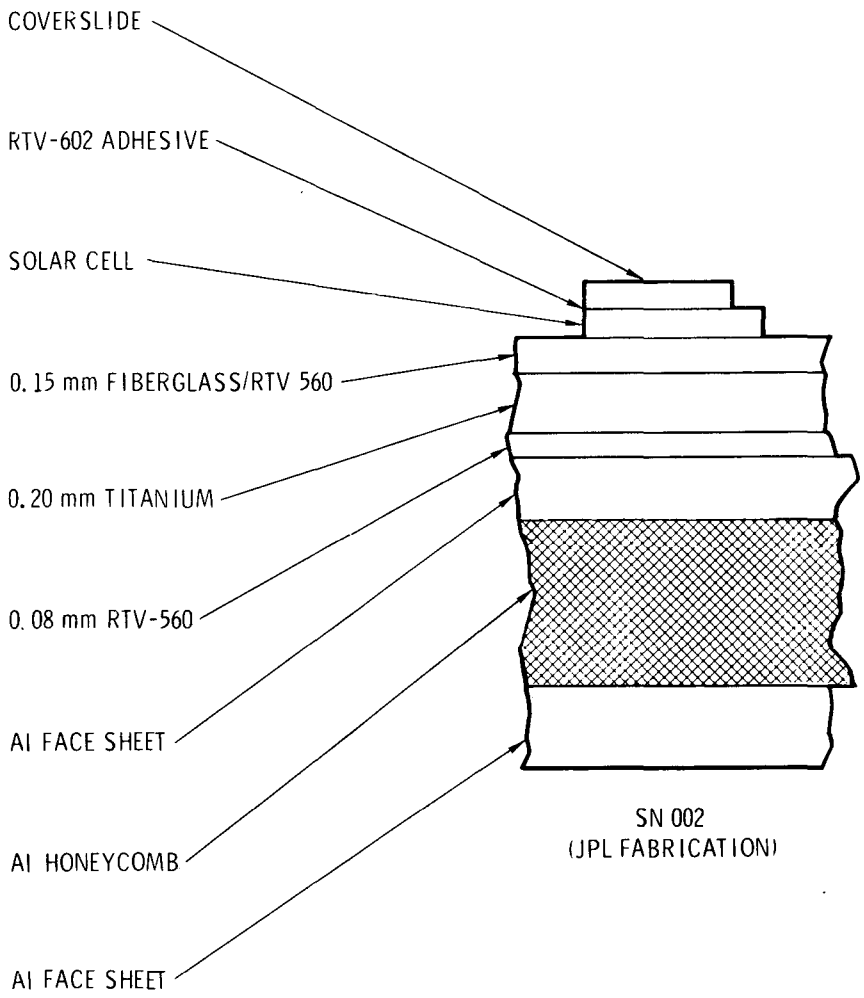

Fig. 4. Cross section of rigid solar panel

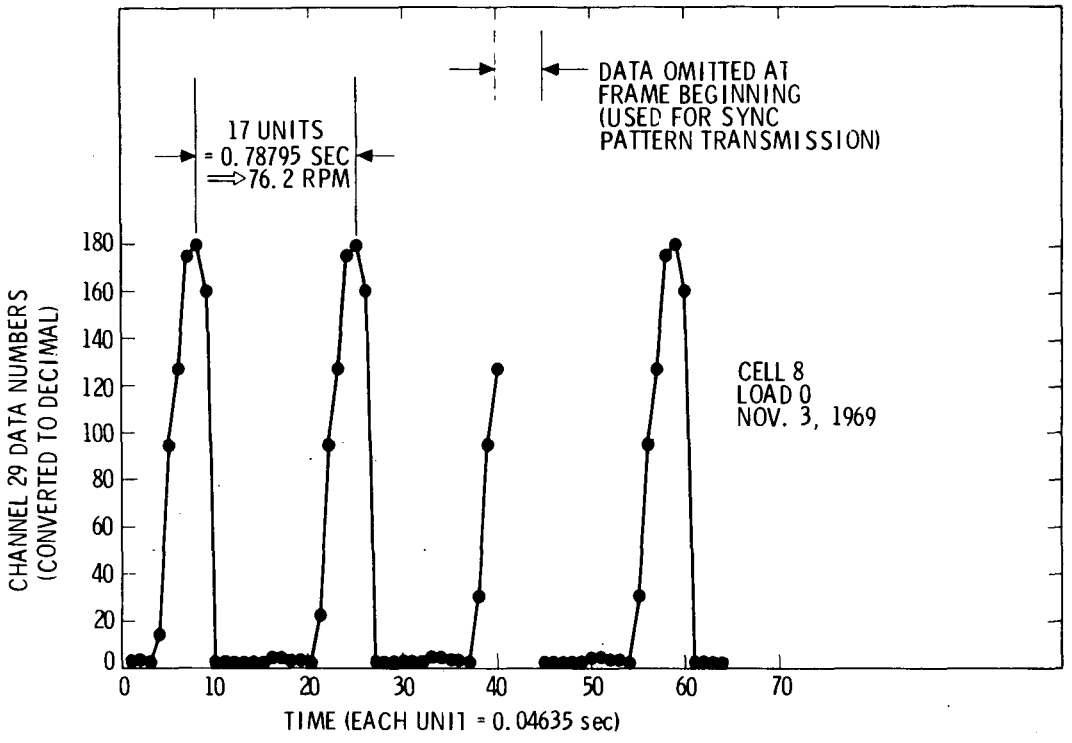

Fig. 5. Voltage channel dwell telemetry data

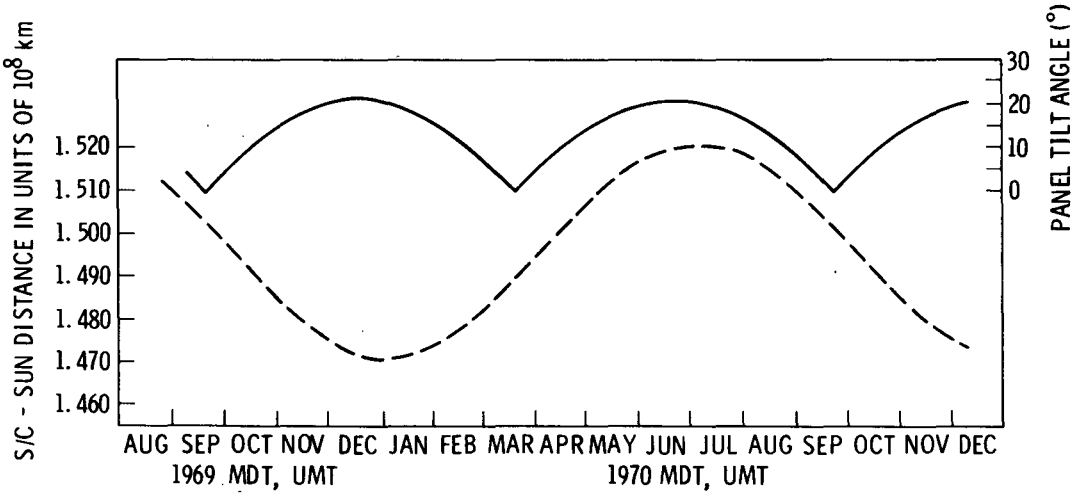

Fig. 6. ATS-5 distance from Sun and spacecraft axis tilt angle vs time

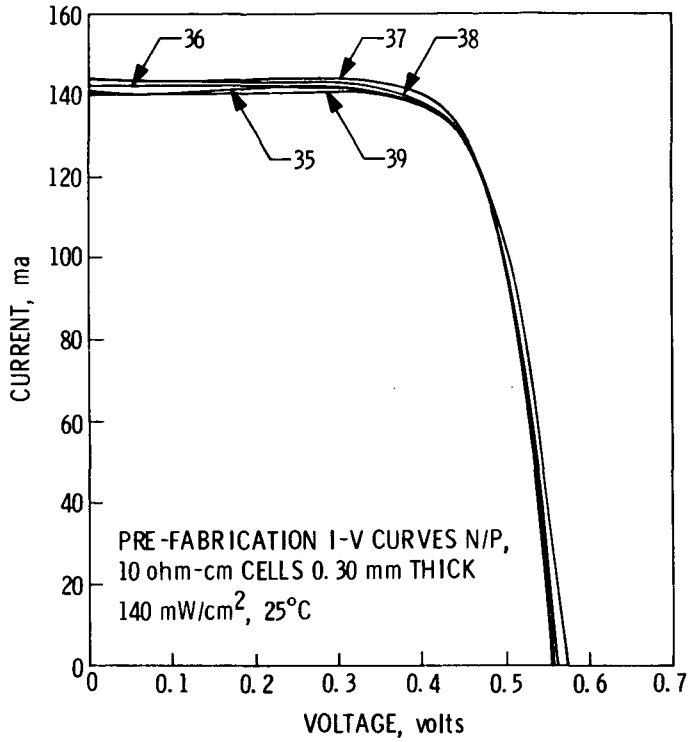

Fig. 7. Prefabrication I-V curves for cells 35-39

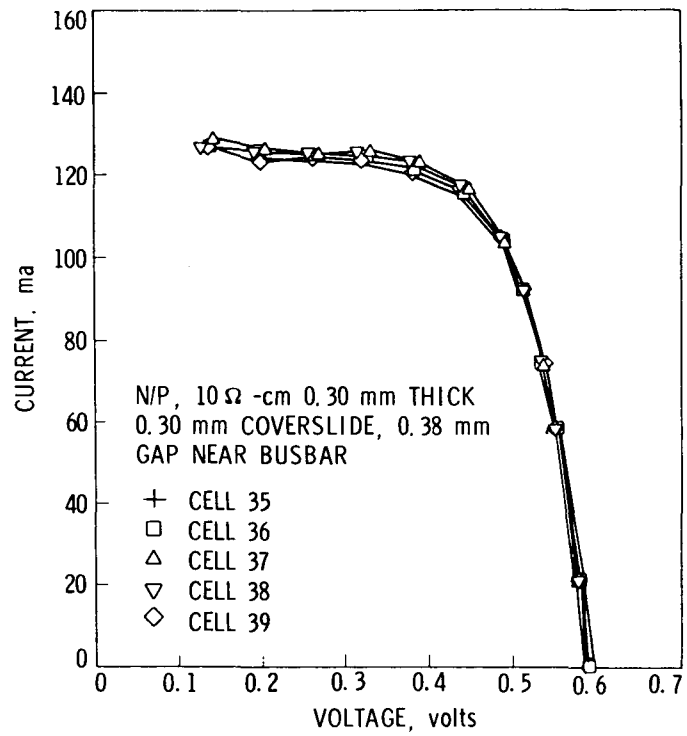

Fig. 8. I-V curves for cells 35-39 after 363 days in orbit

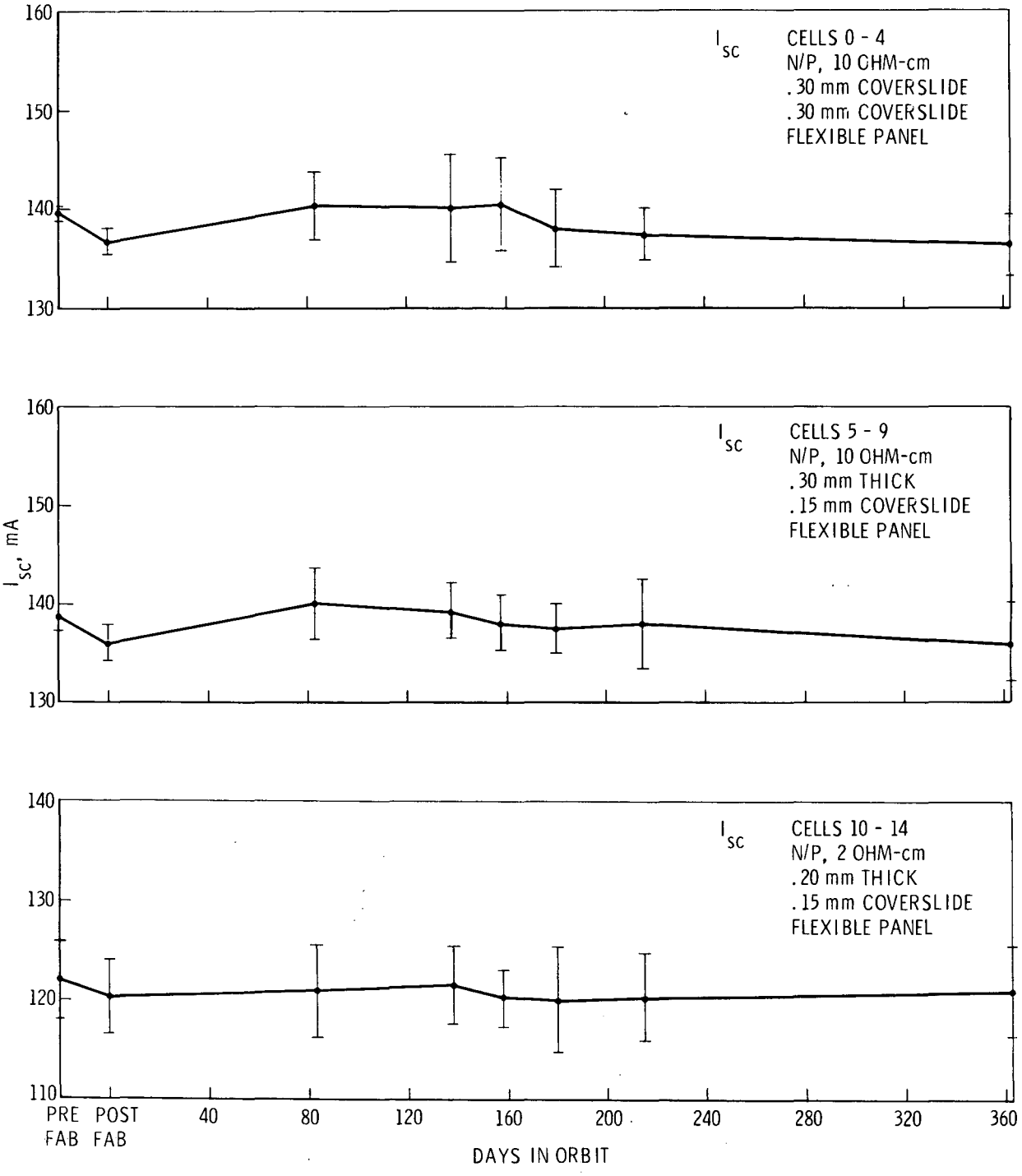

Fig. 9. I_{sc} vs time in orbit for cells 0-14

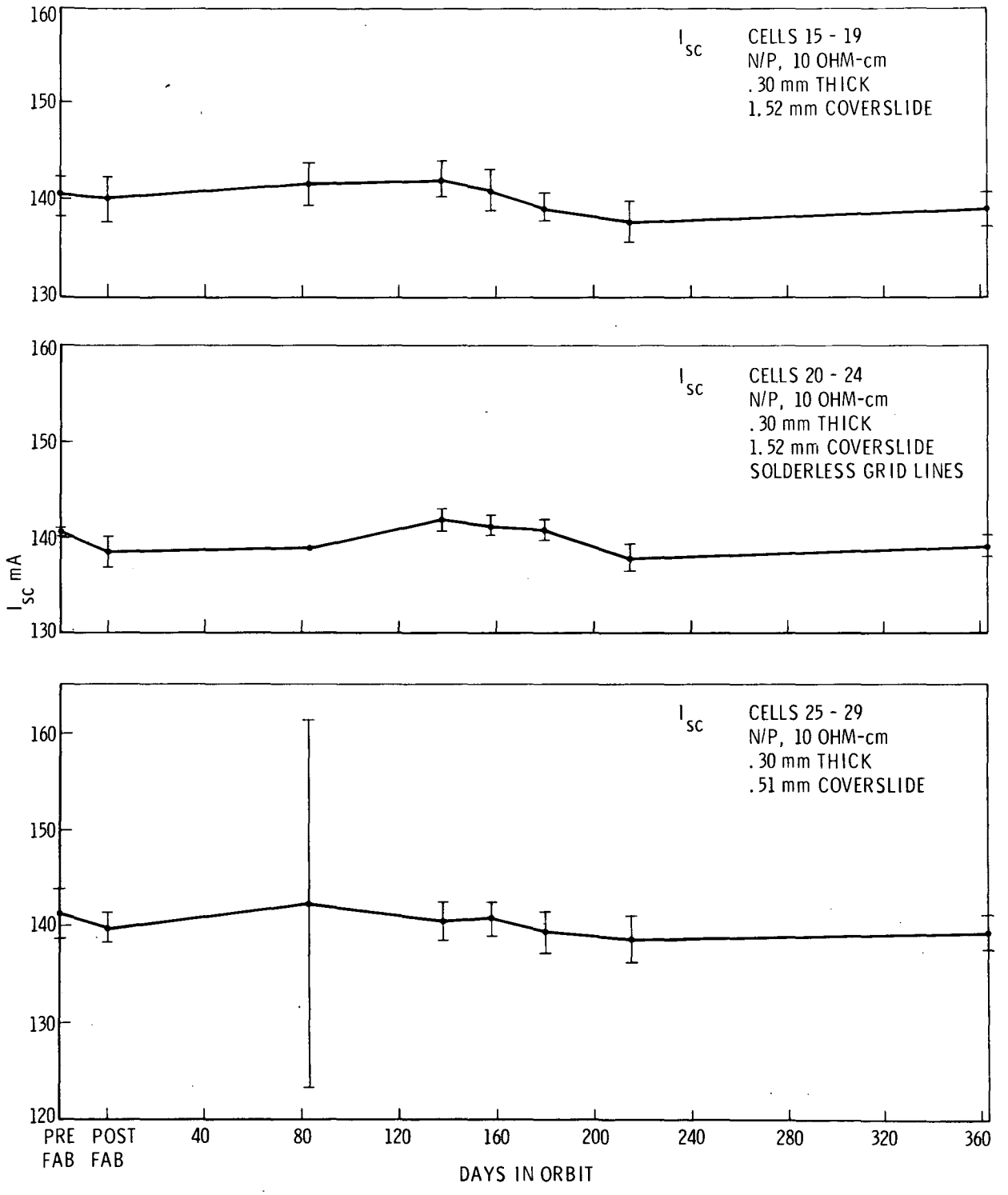

Fig. 10. I_{sc} vs time in orbit for cells 15-29

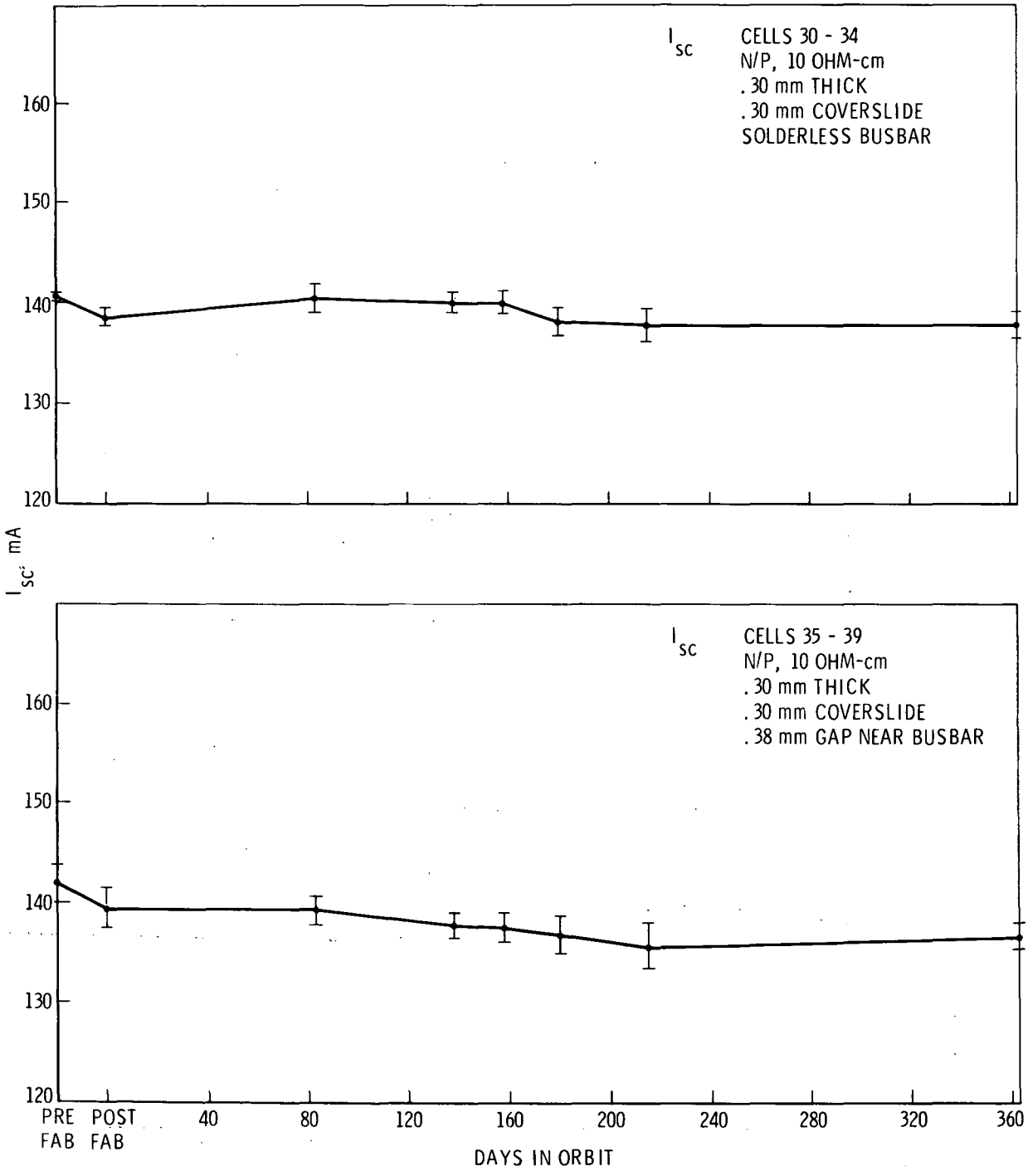

Fig. 11. I_{sc} vs time in orbit for cells 30-39

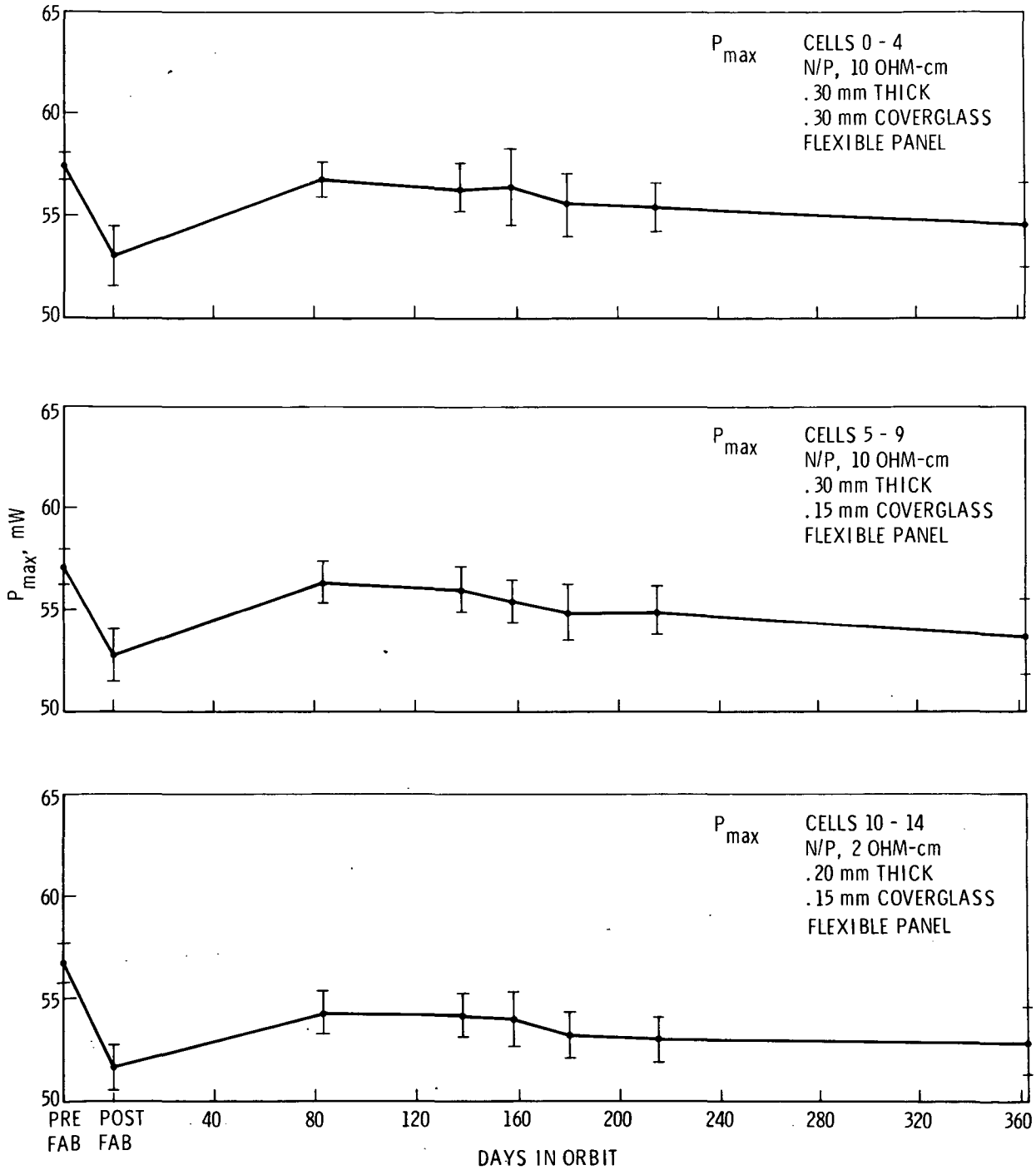

Fig. 12. P_{max} vs time in orbit for cells 0-14

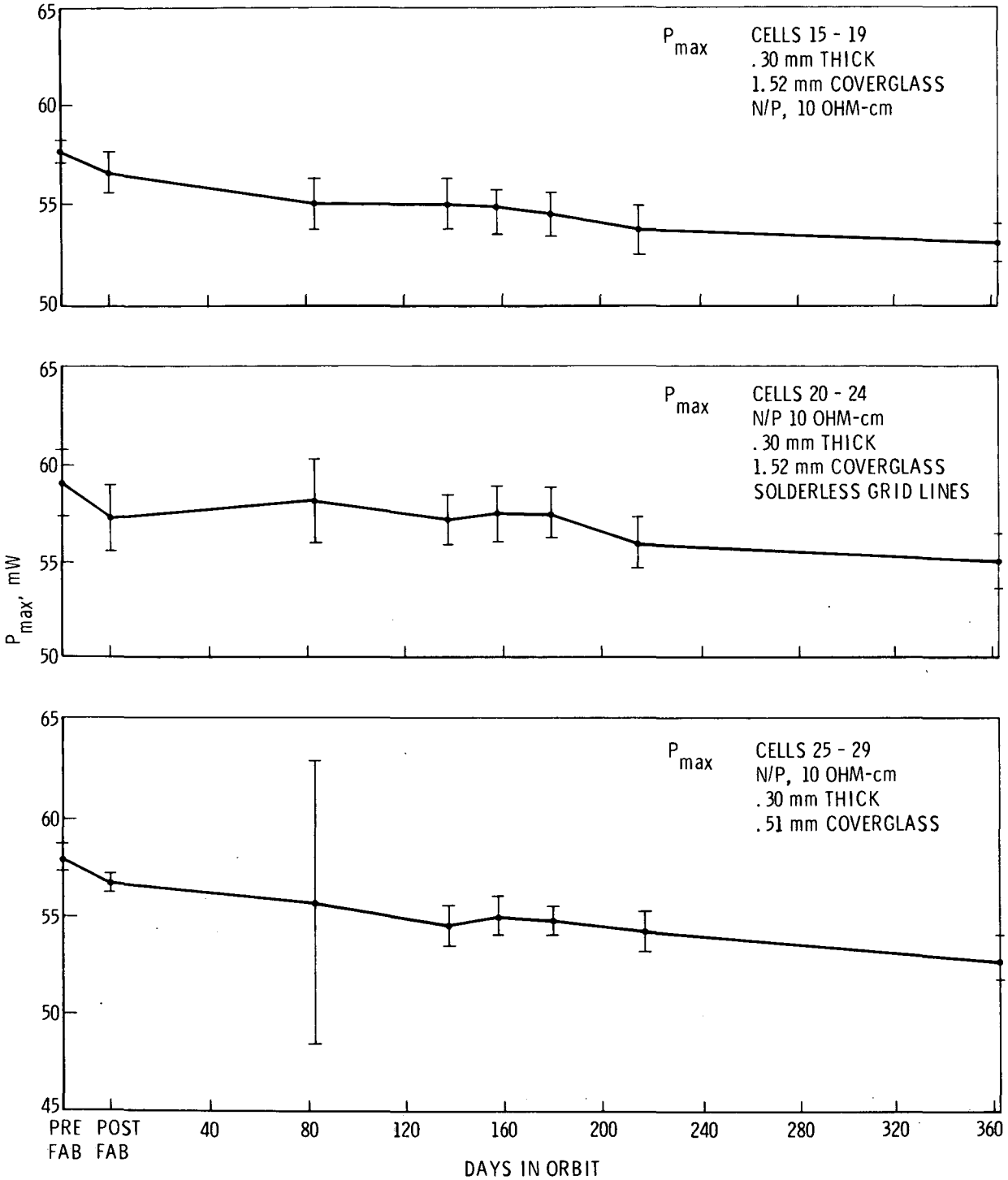

Fig. 13. P_{max} vs time in orbit for cells 15-29

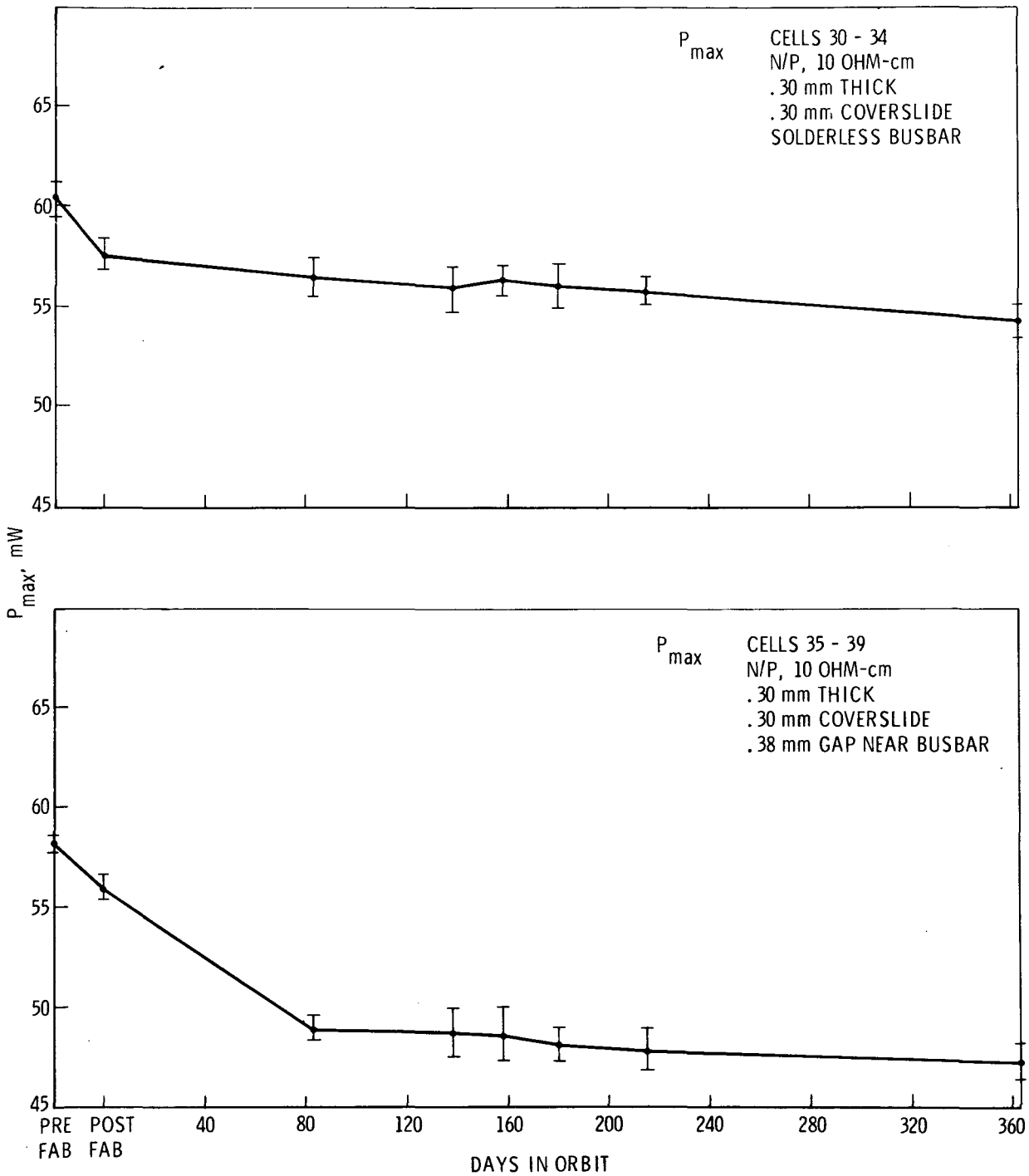

Fig. 14. P_{max} vs time in orbit for cells 30-39

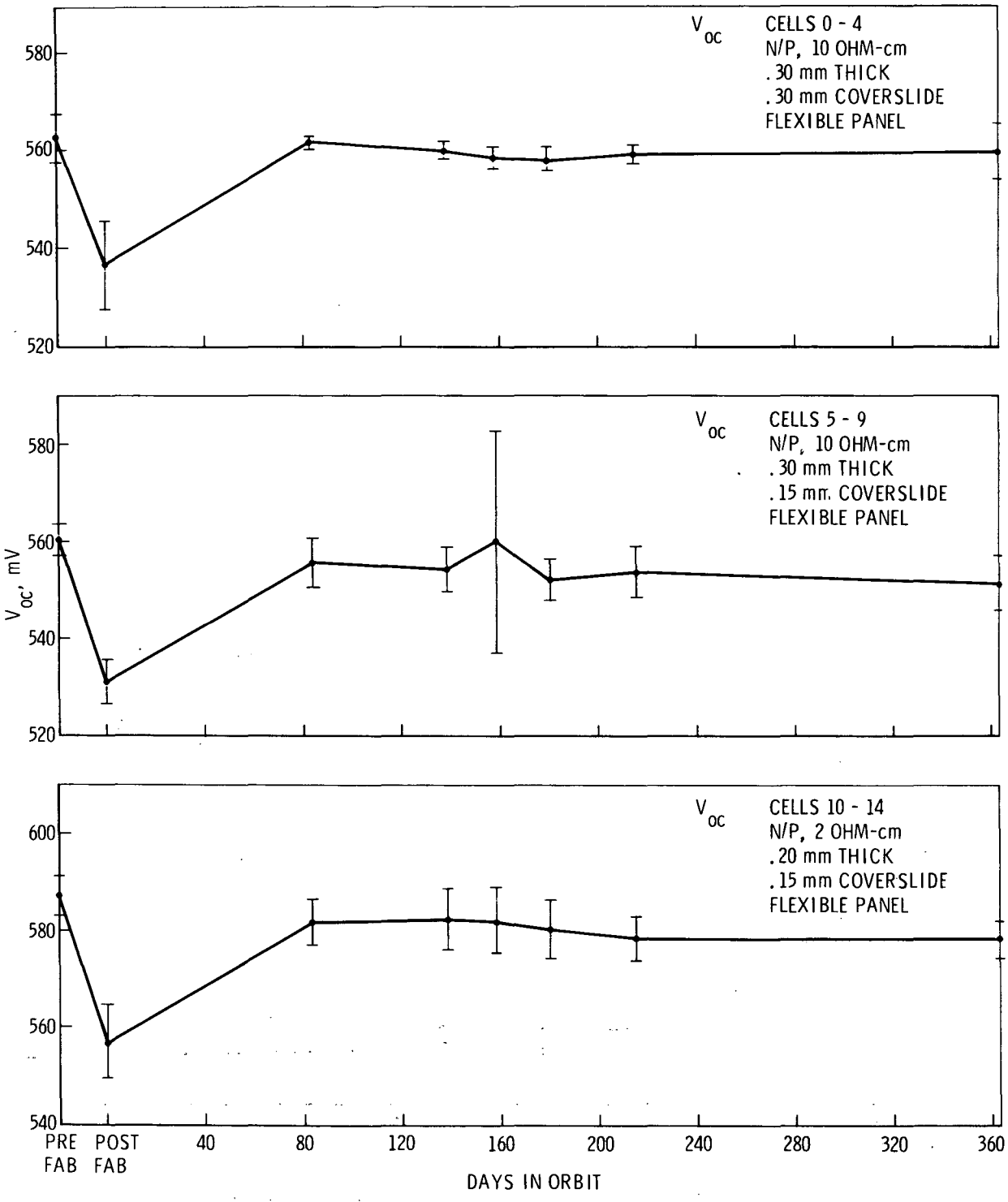

Fig. 15. V_{oc} vs time in orbit for cells 0-14

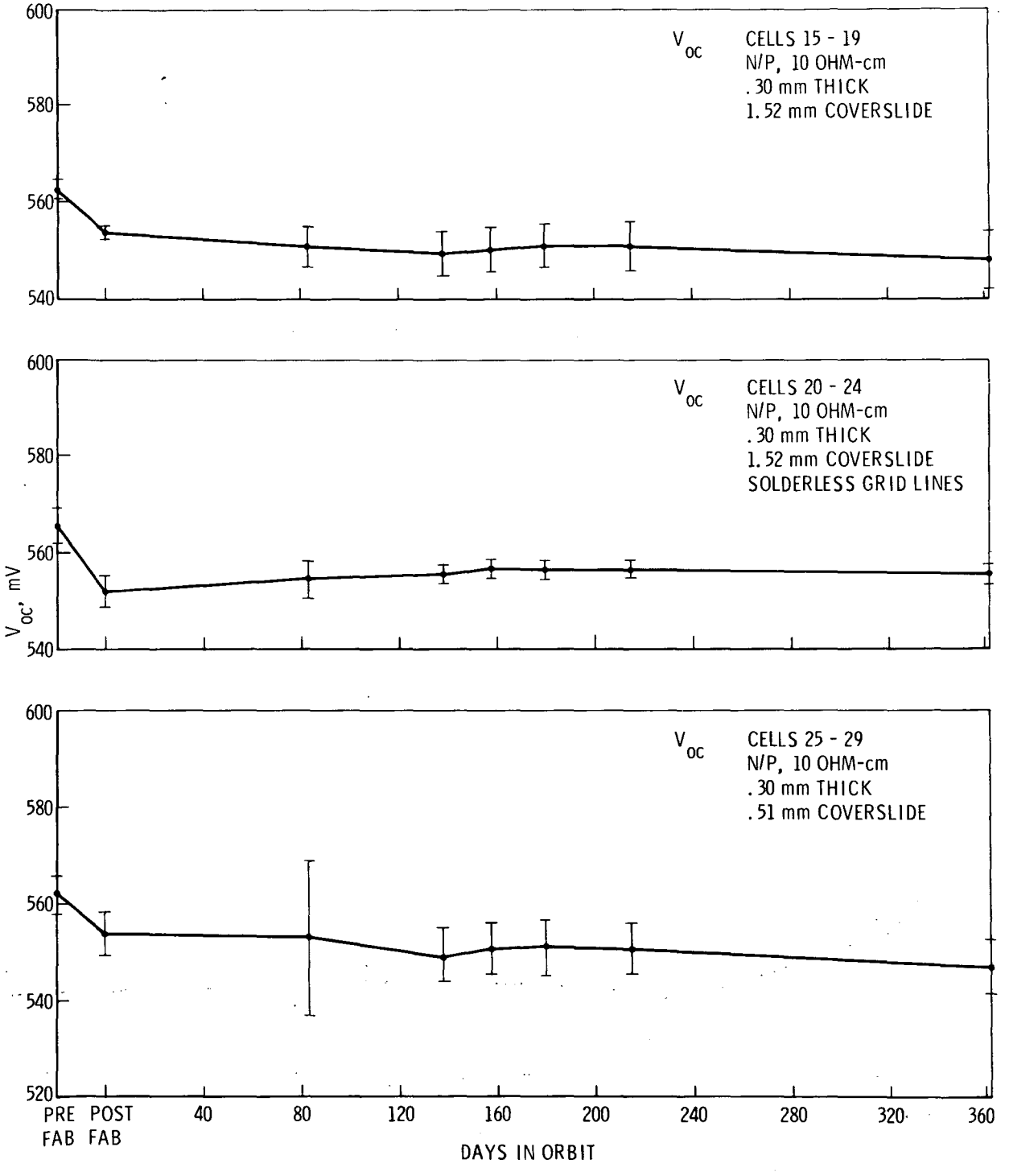

Fig. 16. V_{oc} vs time in orbit for cells 15-29

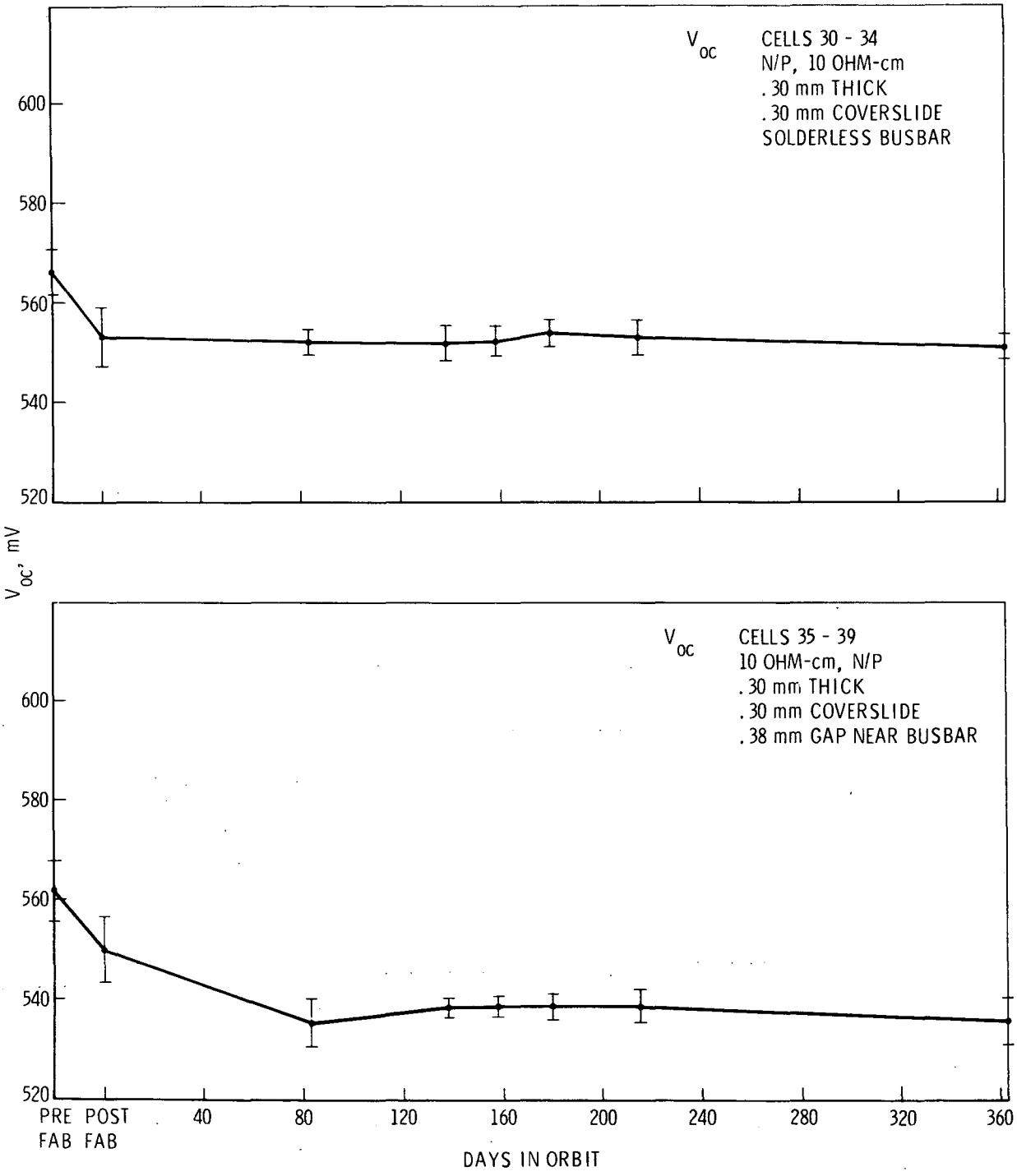

Fig. 17. V_{oc} vs time in orbit for cells 30-39

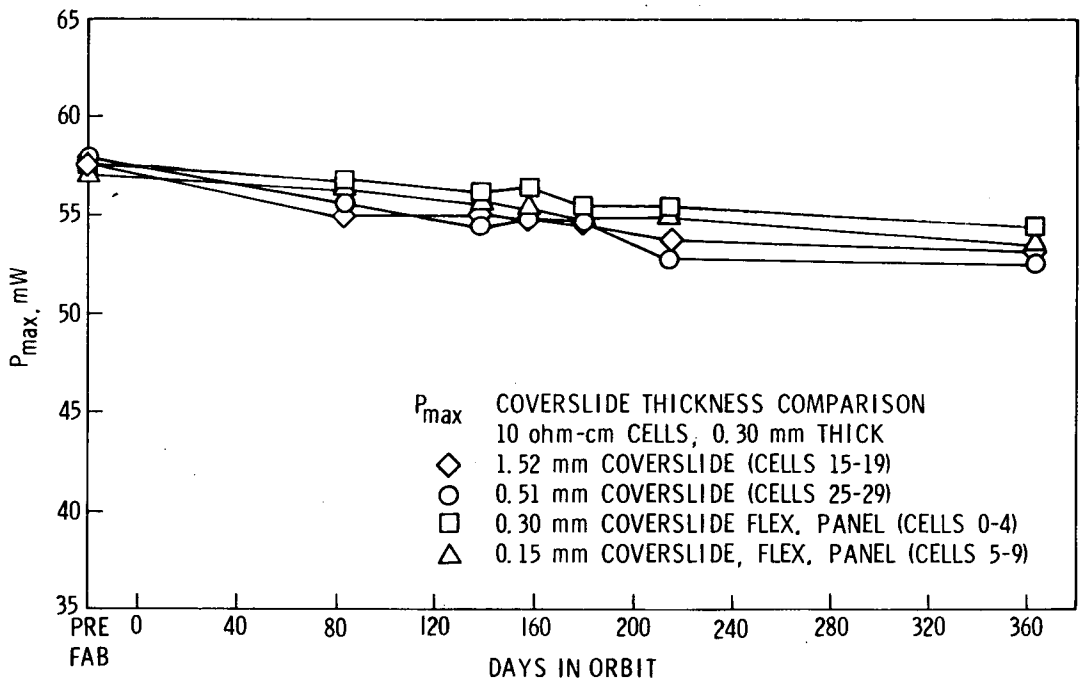

Fig. 18. P_{max} vs time with coverslide thickness as parameter

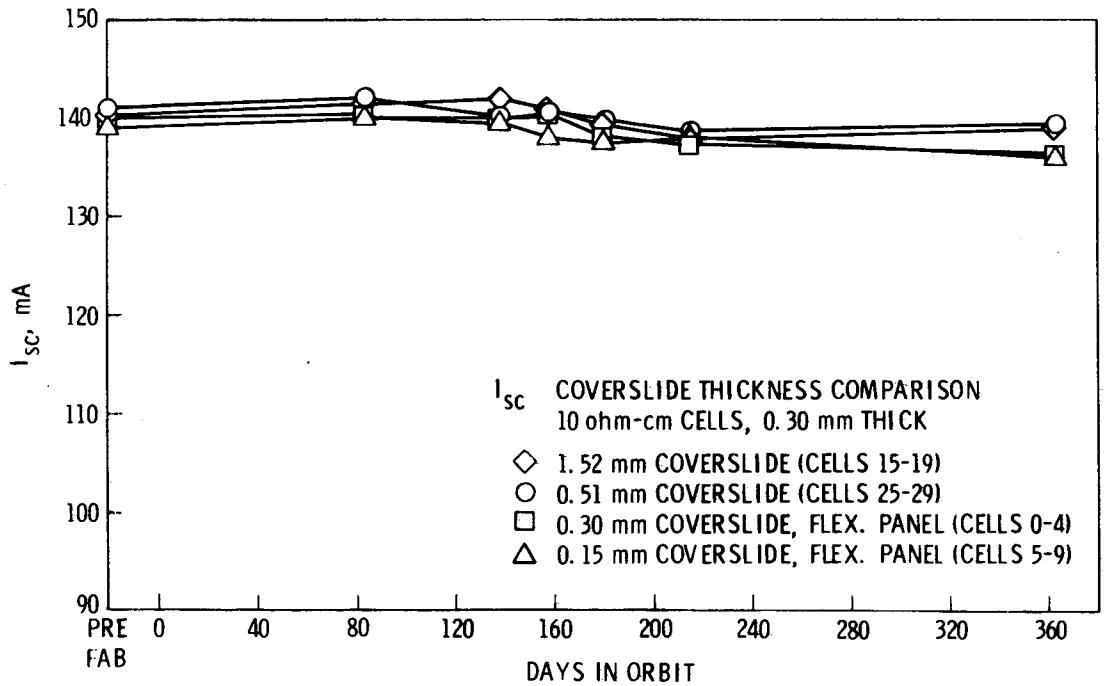

Fig. 19. I_{sc} vs time with coverslide thickness as parameter

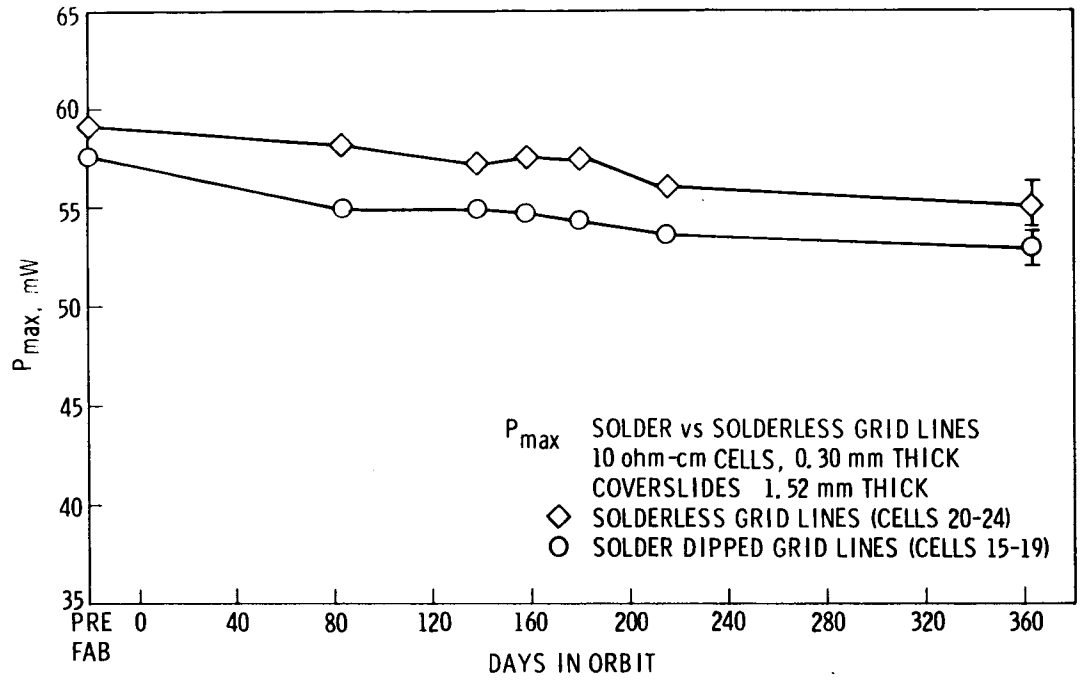

Fig. 20. P_{max} vs time for solder-dipped and solderless grid line cells

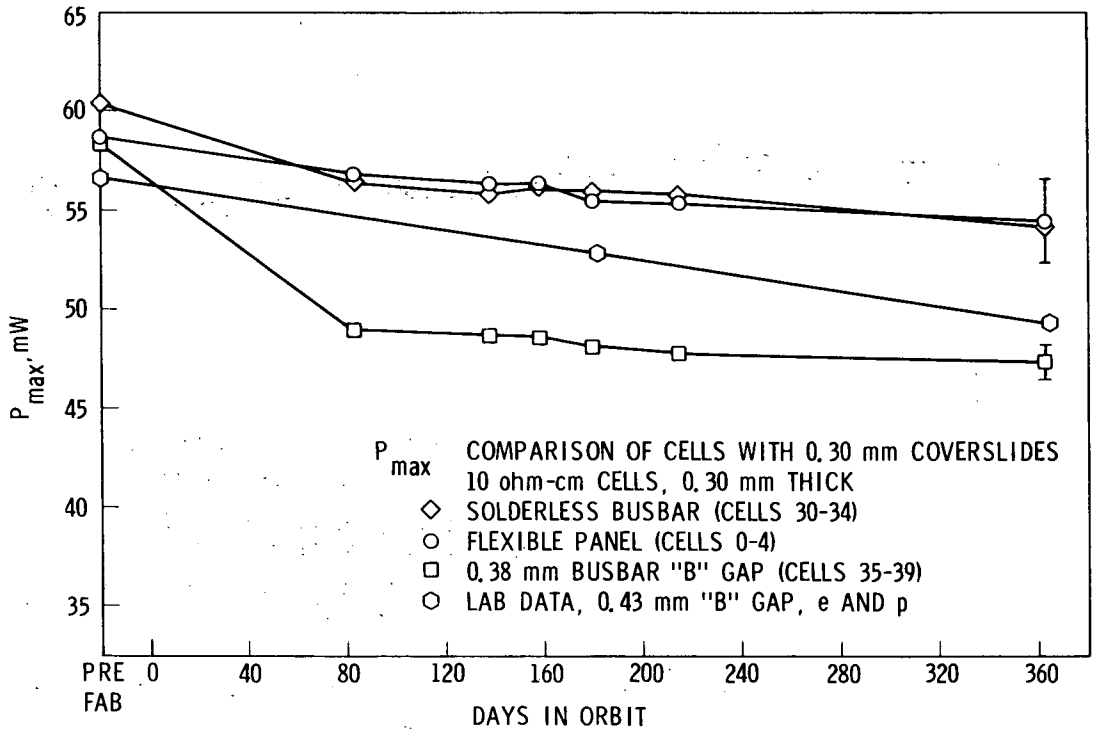

Fig. 21. P_{max} vs time for various 10 Ω-cm cells with 0.30-mm coverslides

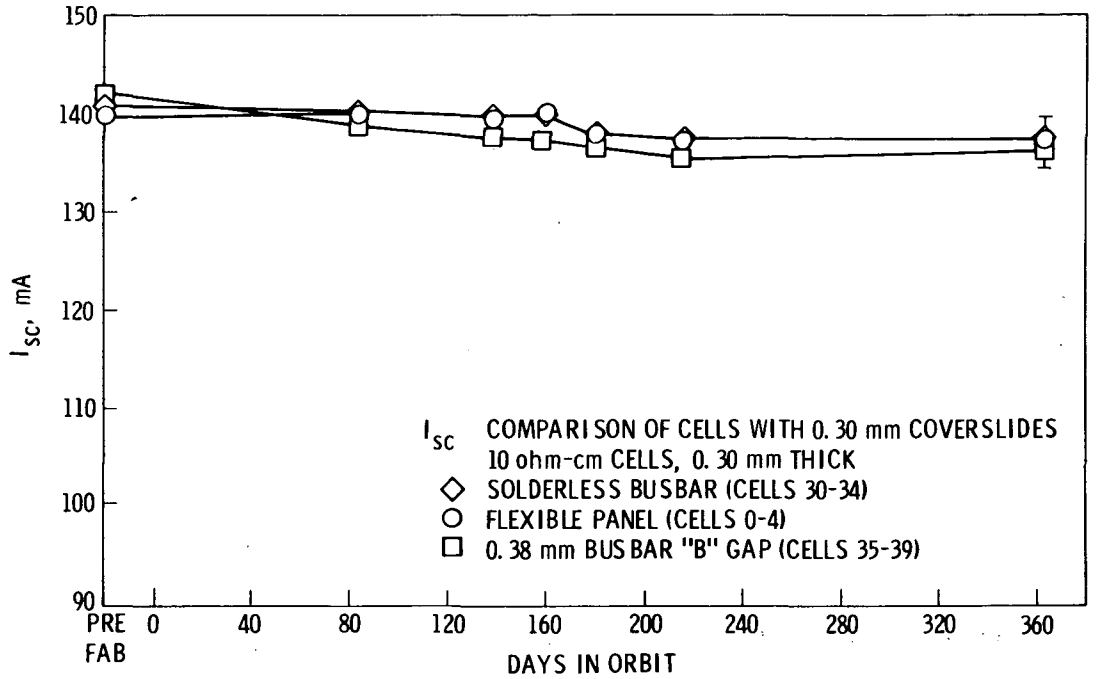

Fig. 22. I_{sc} vs time for various 10 Ω-cm cells with 0.30-mm coverslides

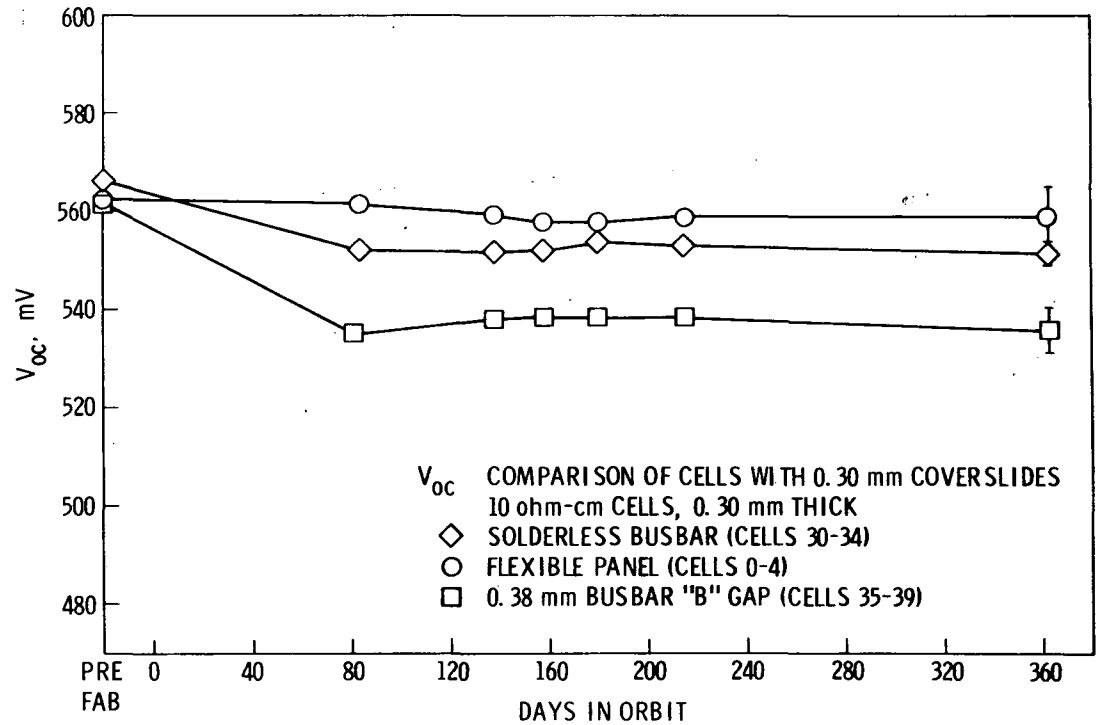

Fig. 23. V_{oc} vs time for various 10 Ω-cm cells with 0.30-mm coverslides

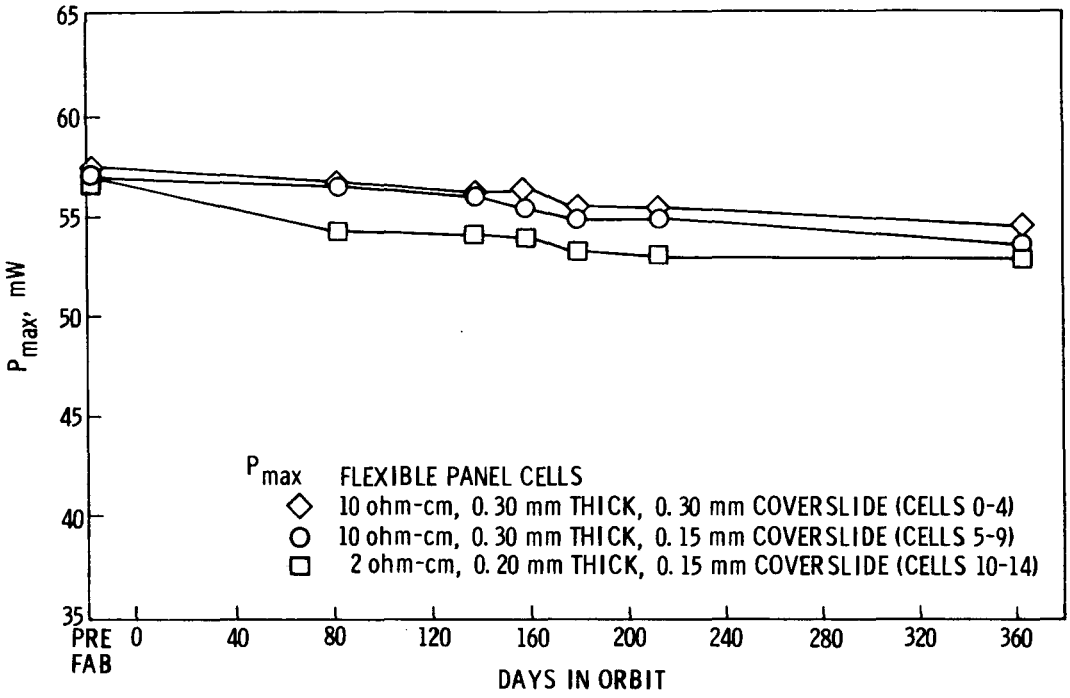

Fig. 24. P_{max} vs time for the cells on the flexible panel

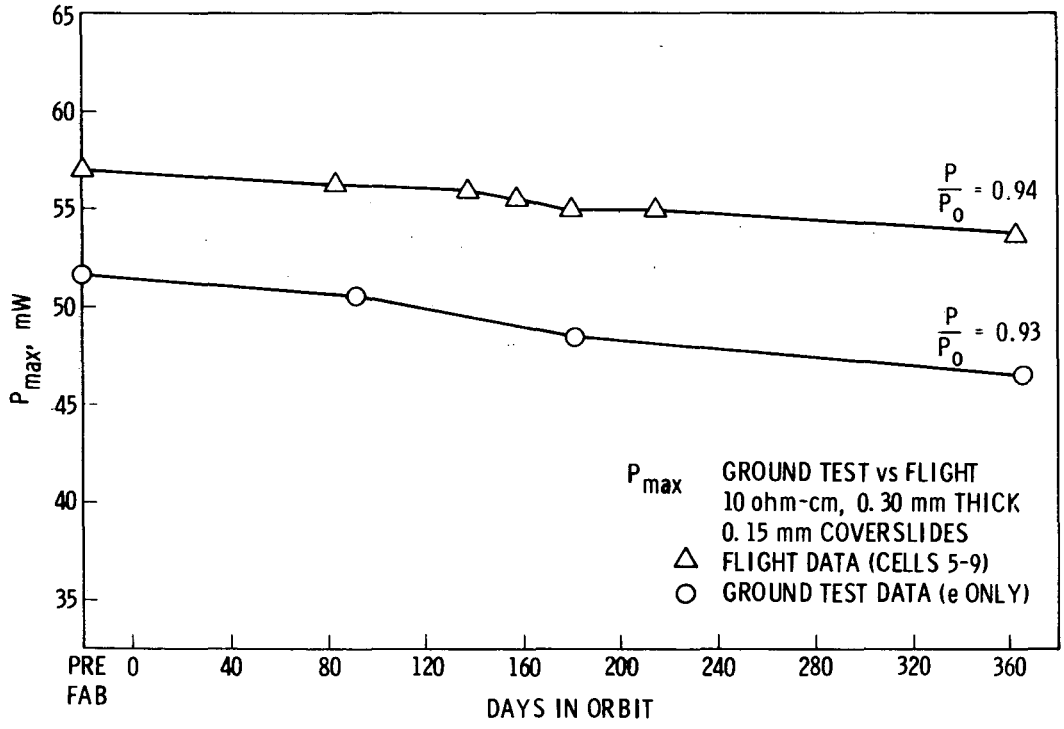

Fig. 25. P_{max} vs time comparing flight vs ground test cells for cells with 0.15-mm coverslides

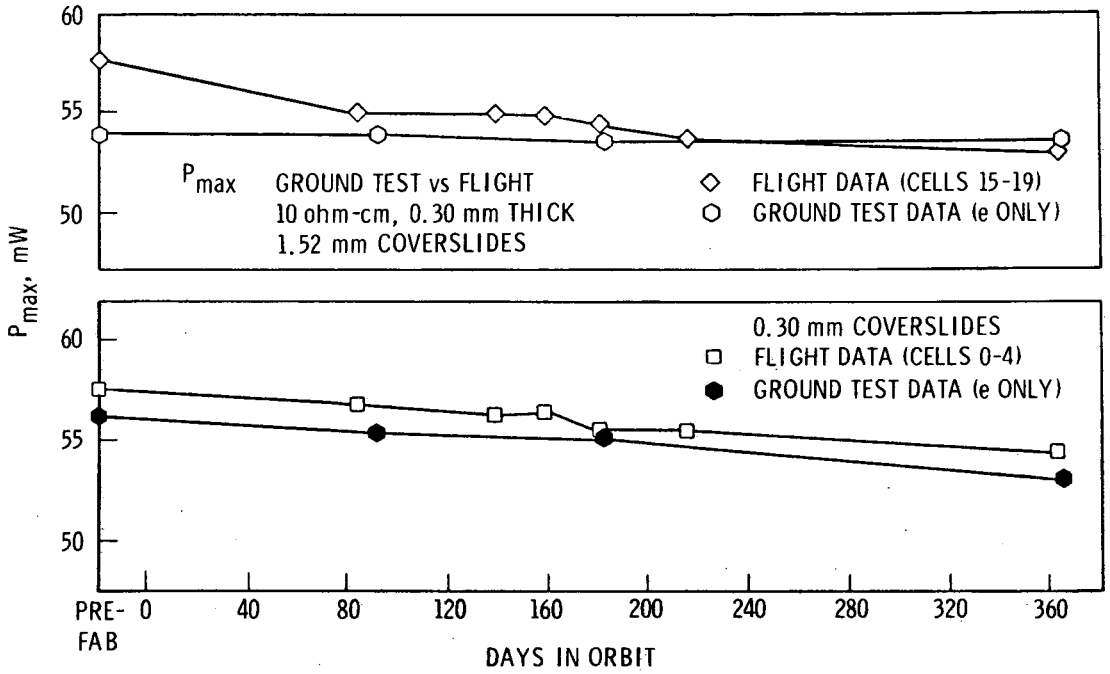

Fig. 26. P_{max} vs time comparing flight vs ground test cells for cells with 1.52-mm coverslides

NASA — JPL — Coml., L.A., Calif.